Contribution of siderite–water interaction for the unconventional generation of hydrocarbon gases in the Solimões basin, north-west Brazil

Vincent Milesi, Alain Prinzhofer, François Guyot, Marc Benedetti, René Rodrigues

CONTRIBUTION OF SIDERITE-WATER INTERACTION FOR THE UNCONVENTIONAL GENERATION OF HYDROCARBON GASES IN THE SOLIMÕES BASIN, NORTH-WEST BRAZIL

Vincent Milesi [*] [a], Alain Prinzhofer [b], François Guyot [c], Marc Benedetti [a] and René Rodrigues [d]

[a] Équipe de Géochimie des Eaux, Institut de Physique du Globe de Paris, Sorbonne Paris Cité, Université Paris Diderot, UMR CNRS 7154, F-75005 Paris, France.

[b] GEO4U. Praia de Botafogo 501, Torre Pao de Açucar, 1° andar, Centro Empresarial Mourisco, Rio de Janeiro, RJ, Brasil CEP 22250-040.

[c] Institut de minéralogie et de physique des matériaux et de cosmochimie, Sorbonne Université. Muséum National d'Histoire Naturelle, UMR 7590, CNRS, UPMC, MNHN, IRD, F-75005 Paris, France.

[d] Universidade do Estado do Rio de Janeiro, Faculdade de Geologia, R. São Francisco Xavier, 524 / sala 2030 A, Maracanã 20550013 - Rio de Janeiro, RJ - Brasil

[*] Corresponding author:

E-mail address: milesi@ipgp.fr (Vincent Milesi)

Abstract

Hydrocarbon gases with unconventional carbon isotopic signatures were observed in the Solimões sedimentary basin in north-west Brazil. Siderite contents measured with a new Rock-Eval methodology in the drill-cuttings samples of the Famenian source rock were found to decrease with the increase of gas maturity and with the occurrence of the gas isotopic anomalies. Triassic diabase intrusions induced heating of the source rock, which likely

resulted in the gradual oxidative dissolution of siderite as suggested by the observation of etch pits on the siderite surfaces. It is proposed that ferrous iron from the carbonate was involved in a redox reaction with water producing ferric iron and H_2, then reducing CO_2 and yielding an inverse correlation between siderite content and gas maturity. Alternatively, hydrogenation of highly mature kerogen by H_2 derived from siderite could explain the production of ^{13}C-rich CH_4. Mass balance considerations suggest that these mechanisms may account for a significant fraction of the hydrocarbon gases generated from the Famenian source rock in the Solimões basin.

1. INTRODUCTION

Natural hydrocarbons are most often formed either by microbial processes (Whiticar *et al.*, 1986), or by thermal decomposition of organic matter following a kinetic law dependent on both time and temperature (Tissot *et al.*, 1987). Both processes lead to an isotopic fractionation of the produced hydrocarbons with respect to their source, due to the preferential breaking of bounds containing ^{12}C (Des Marais *et al.*, 1981). Thereby, thermal generation of hydrocarbons results in an enrichment of the products in ^{12}C, i.e., a decrease of the $\delta^{13}C$ with a decrease in carbon number (Chung *et al.*, 1988; Prinzhofer and Huc, 1995). This implies that there is a so-called "normal isotopic trend" for hydrocarbon gas compounds, with $\delta^{13}C_1 < \delta^{13}C_2 < \delta^{13}C_3 <\ldots$ where C_1, C_2 and $C_3\ldots$ stand for the number of carbon atoms in the molecule.

Increasing demand for natural gas has led petroleum exploration toward unconventional gas accumulations such as tight gas sands, fractured reservoirs, coalbed methane and shale gas. Reversal from the normal sequence of isotopic compositions ($\delta^{13}C_1 > \delta^{13}C_2 > \delta^{13}C_3$) has been reported in few conventional gas accumulations, but becomes more

common in unconventional accumulations (e.g., Jenden *et al.*, 1993; Laughrey and Baldassare, 1998; Burruss and Ryder, 2003; Dai *et al.*, 2004, 2005). In shale gas accumulations, isotopic inversion has been proposed to be a fair indicator of the quality of the resource (Tang and Xia, 2010; Zumberge *et al.* 2012).

Reversals in isotopic compositions can result from different processes such as the oxidative destruction of hydrocarbon gases by either thermochemical sulfate reduction (Krouse *et al.*, 1988) or microbial activity (James and Burns, 1984; Hunkeler *et al.*, 1998; Katz *et al.*, 2011), or the mixing between gases from sources at different levels of maturity and different origins including abiotic sources (Jenden *et al.*, 1993; Dai *et al.*, 2004, 2008; Huang *et al.*, 2004; Xia *et al.*, 2013). Prinzhofer and Huc (1995) showed that isotopic reversals can also be explained by partial diffusive leakage from gas reservoir involving the most diffusive molecules, i.e., the ^{13}C-depleted compounds. Rayleigh fractionation of ethane and propane driven by redox reactions with transition metals and water at high temperatures (> 250°C) were proposed by Buruss and Laughrey (2010) to explain the isotopic inversions reported in hydrocarbons from the northern Appalachian basin.

During the study of mineral exploration boreholes in crystalline Precambrian rocks, Sherwood Lollar *et al.* (2002, 2006) reported alkanes presumably generated from abiotic processes showing $\delta^{13}C_1 > \delta^{13}C_{2\text{-}4}$. Such patterns could result from kinetically controlled synthesis of high-molecular-mass alkanes from smaller ones (polymerization) in which the lighter $^{12}CH_4$ reacts faster than the heavier $^{13}CH_4$ to be incorporated into larger hydrocarbon chains (Des Marais *et al.*, 1981; Yuen *et al.*, 1984). To explain abiogenic gas production, Sherwood Lollar *et al.* (2002, 2006) suggested either heating or metamorphism of graphite-carbonate-bearing rocks (Giardini *et al.*, 1968; Holloway, 1984), or a Fischer-Tropsch-Type process, consisting of surface catalyzed reduction and polymerization of CO or CO_2 into CH_4 and larger hydrocarbon gases. Abiotic generation of hydrocarbons through the Fischer-

Tropsch-Type process is commonly evoked in geothermal systems associated with ultramafic rocks at mid-oceanic ridges (e.g., Holm and Charlou, 2001; Kelley *et al.*, 2001; Charlou *et al.*, 2002) or in ophiolites (e.g., Abrajano *et al.*, 1988; Hosgormez *et al.* 2008; Etiope *et al.*, 2011). In this context, the serpentinization of olivine induces the production of H_2-rich fluids from redox reactions between ferrous iron and water:

$$Fe^{2+}_{(Olivine)} + H_2O \rightarrow Fe^{3+}_{(Magnetite)} + OH^- + 0.5\ H_2 \quad (1)$$

The produced H_2 subsequently reduces the CO_2 transported in the hydrothermal fluids to produce hydrocarbons including CH_4. In fluids from the Lost City hydrothermal vents, Proskurowski *et al.* (2008) report the formation of alkanes from C_2 to C_4 depleted in ^{13}C relative to CH_4. Polymerization of light $^{12}CH_4$ into longer alkanes during a Fischer-Tropsch-Type process was proposed to explain the inverse isotopic trend.

The generation of H_2- and CO_2-rich fluids enabling the Fischer-Tropsch-Type process can also be achieved through reaction between water and siderite ($FeCO_3$). Experimental decomposition of siderite in the presence of vapor at 300°C by McCollom (2003) produced mainly magnetite along with CO_2 and H_2 in the gas phase. Small amounts of organic compounds including CH_4 also formed suggesting an overall reaction written as

$$\underset{\text{siderite}}{3\ FeCO_3} + w\ H_2O_{(l)} = \underset{\text{magnetite}}{Fe_3O_4} + x\ CO_{2(g)} + y\ CO_{(g)} + z\ H_{2(g)} + \underset{\text{compounds}}{\text{organic}} \quad (2)$$

(McCollom, 2003), where *w*, *x*, *y* and *z* are stoichiometric coefficients. Milesi *et al.*, 2015 conducted laboratory experiments between siderite and water in gold containers at 200-300°C and 50 MPa, which yielded mostly magnetite, condensed carbonaceous material, CO_2, H_2 and CH_4. Thermodynamic calculations indicate that CO_2 and H_2 are close to equilibrium with the siderite – magnetite – graphite mineral assemblage and that CH_4 can be produced by reduction of CO_2. In nature, siderite has been invoked to explain the occurrence of reduced

carbon in metamorphic rocks (e.g., Perry and Ahmad, 1977; Ueno *et al.*, 2002). van Zuilen *et al.* (2003) suggested that, in the carbonate-rich metasomatic rocks of the 3.8 Ga Isua Supracrustal Belt (Greenland), the presence of graphite was due to thermal decomposition of siderite. Zolotov and Shock (2000), McCollom (2003) and Steele *et al.* (2012) also proposed the decomposition of Fe-bearing carbonate as a source of reduced carbon in Martian meteorites.

In the present work, hydrothermal dissolution of siderite is proposed to generate hydrocarbon gases with unconventional carbon isotopic signature in the Solimões sedimentary basin in north-west Brazil. Hydrocarbon gases show inverse isotopic trends in the western part of the study area, which experienced high paleo-temperatures (see discussion below) related to magmatic activities. The Solimões basin was studied in terms of redox conditions in the source-rocks through the characterization and quantification of the iron-rich mineral phases. In this framework, the Rock-Eval instrument was used with a new methodology (Pillot *et al.*, 2014) to characterize and quantify the different carbonates in rock samples.

2. REGIONAL GEOLOGIC SETTING

The Solimões basin is a large, east-west trending, Paleozoic cratonic depression covering an area of approximately 450,000 km^2 of the Amazonas State, northern Brazil (Fig. 1a, modified from Elias *et al.*, 2004). It is limited to the south and north by the Brazilian and Guiana shields, respectively. It is surrounded by the Iquitos Arch of the Acre basin to the west and by the Purus Arch of the Amazon basin to the east. The Solimões basin is divided by the north-south Carauari Arch into two sub-basins: the Jandiatuba sub-basin, in the western area,

and the Juruá sub-basin, in the eastern area. Our study focused on the Juruá sub-basin (Fig. 1a).

The tectonic origin of the Solimões basin is under debate. One of the most recent hypotheses suggests that the origin and regional subsidence of the basin occurred in a flexural regime, progressing towards the east, and that it was related to rifting parallel to the western margin of Gondwana during the Ordovician. Basin formation would have become effective during thermo-mechanical subsidence after that rifting stage, synchronous with the formation of other interior sag and marginal basins (Campos *et al.*, 1991).

The Proterozoic basement of the Solimões basin consists of igneous and metamorphic rocks. The Juruá sub-basin is filled with almost 4,000 m of sediments ranging from an Upper Proterozoic, siliciclastic sequence deposited in a rift system, to a Quaternary sequence of siliciclastics (Fig. 1b; modified from Eiras *et al.*, 1994). The most important sedimentary sequence is represented by Paleozoic sediments that host a petroleum system, i.e., the Jandiatuba-Juruá formations (Eiras, 1998a). The source rocks are represented by the Upper Devonian marine black shale (Jandiatuba Formation) that can reach a thickness of 40 m with total organic carbon reaching 4 wt.% and vitrinite reflectance (Ro) more than 1% in the northern part of the study area (Eiras, 1998a). Recently, a series of 10 exploratory wells drilled by the HRT Oil and Gas Company (Fig. 1a) showed that the Devonian source rock had three producing intervals of Givetian, Frasnian and Famenian ages. In the study area, the Givetian source rock is not much present, whereas the Frasnian and Famenian source rocks are much more expanded and reach thicknesses of up to 50 and 60 m, respectively (Fig. 2a). Because of magmatic intrusions peculiarly close to the source rock in the study area, all the organic matter shows extremely high maturity, at the end of the gas window, rendering any source characterization quite difficult. However, paleogeographic reconstruction and comparison with the source rocks from the Amazonas basin (Gonzaga *et al.*, 2000) suggest

that the Famenian source rocks correspond to a regressive phase representing shallow water and periglacial formations (diamictite). This results for the Famenian in a more gas-prone source-rock whereas the Frasnian black shale contains oil-prone marine type-II kerogen. The gas-prone character of the Famenian source rock suggests a depositional environment less reduced than that of the Frasnian shale, which is supported by a lower total organic carbon (TOC) in the Famenian formation than in the Frasnian shale (Fig. 2b). Indeed, the maximum TOC of the Famenian source rocks is of ~2 wt.% located to the north of the study area whereas the Frasnian formation shows a maximum TOC of ~3 wt.% further east (Fig. 2b). In exploratory wells A, B, C and D, the TOC in the Famenian formation is relatively constant ~1 wt.%, whereas it ranges from 1 to 3 wt.% in the Frasnian shale (Fig. 2b). During exploration, the temperature in the source rock was measured at ~100°C and the pressure was estimated to be ~30 MPa.

The best reservoir rock of the petroleum system is represented by sandstones of the Juruá Formation that can reach up to 50 m, and were deposited during the Late Carboniferous under eolian, tidal plain and shallow marine conditions (Caputo and Silva, 1990). Sealing is provided by evaporites (anhydrite and halite) found at the base of the Pennsylvanian Carauari Formation. The classical trapping style in the Solimões basin is fault propagating folds formed by dextral wrenching during the Late Jurassic to Early Cretaceous period (Figueiredo and Milani, 2000).

The Jandiatuba-Juruá petroleum system is unusual because thermal maturation of the source rocks was significantly enhanced by Late Triassic to Early Jurassic igneous intrusions (Mosmann *et al.*, 1987; Rodrigues *et al.*, 1991). Such diabase sills are clustered in at least three groups of intrusive bodies concordant with the lithostratigraphic horizons for large areas (Fig. 1b). In the study area, three dolerite sills are present in the west, whereas two are present in the central area and are more distant from the petroleum system (Fig. 1b). According to the

location of Well A, B, C and D (Fig. 1b), thermal effects induced by the magmatic intrusion increased from Well A to Well D. Going South, the dolerite sills disappear, either due to erosion, or that magmatic activity did not reach this area.

A possible scenario of petroleum generation is that traps were formed in the Paleozoic and petroleum began to be produced during the Carboniferous as a result of deep burial with a transformation ratio of 50% (Eiras, 1998a). Heating induced by the Triassic diabase intrusions led to the decrease in the petroleum potential of the source rocks to zero, and to severe secondary cracking where the lower dolerite sill is close to the source rocks (Eiras, 1998a). The gas accumulations are concentrated in the overmature areas in the western part of the basin (vitrinite reflectance Ro > 1.35%), whereas light oil and condensate have been found in areas with relatively lower thermal effects in the eastern part (Mello *et al.*, 1994). More recent studies based on the relationship between the abundance of diamondoids and steranes in oils and 3D-modeling have shown that the heat from igneous intrusions contributed significantly to the secondary hydrocarbon cracking within reservoirs (Freitas *et al.*, 2000; Bender *et al.*, 2001). Post-magmatic tectonism may have caused remobilization of the former hydrocarbon accumulations and caused significant losses during hydrocarbon remigration (Murakami *et al.*, 1993).

3. MATERIALS AND METHODS

Formation water and gas samples are from 10 exploratory wells drilled by the HRT Oil and Gas Company. They were collected during drill tests, which were designed to sample the formation fluids (gas, oil and water) and to prevent contaminations by the drilling mud. Water samples were kept away from ambient atmosphere and light to minimize oxidation. Centrifugation was used to remove impurities before analysis. For gas samples, the

headspaces of the drill tests were directly injected to the gas chromatograph. Gas samples were analyzed less than 48 hours after sampling.

Rock samples are from the exploratory wells A, B, C and D (Fig. 1). The rock samples are recovered from the drill-cuttings samples, which are made of crushed formation rock mixed with drilling mud. The drill-cuttings samples were washed three times with soap, then rinsed and sieved to 200 μm under a water flow, before being dried at 50°C during 24 h. The sample collection ranges from the Carboniferous reservoir to the Devonian source rock.

Gas analyses were performed at the IPEXCo laboratories with a gas chromatograph connected to two thermal conductivity detectors and a flame ionization detector, allowing quantification of CO_2, O_2, N_2, He, H_2 and all hydrocarbons from methane to iso- and normal-butane. Individual hydrocarbons were separated by on-line gas chromatography and their isotope-ratios were measured by mass spectrometry. Isotopic compositions are reported relative to the Peedee belemnite (PDB) standard for carbon. Precisions for individual components concentrations in the molecular analysis are ± 5% and ± 0.5‰ for $\delta^{13}C$.

The water samples were analyzed with ion chromatography and inductively-coupled plasma associated with a mass-spectrometer (ICP-MS) to measure major anions, cations and dissolved metals at the laboratory of Geochemistry of UERJ. Before analysis, the water samples were diluted with 2% HNO_3 solution. The measurements of the cation and anion concentrations in the water samples show contamination by drilling mud. The end-member compositions of the formation waters and of the drilling mud were characterized using mixing diagrams. The water samples showed sulfate concentrations one to two orders of magnitude lower than drilling mud. Thus, the sulfate concentrations in the formation water were approximated to be null relative to those in drilling mud. Concentrations of major cations were plotted as function of SO_4^{2-} concentrations (figure not shown), and end-member

concentrations of Solimões waters were calculated by linear regression of drilling mud and samples compositions to zero sulfate. Error bars for end-member concentrations are ±20%. The extent of drilling mud contamination was roughly quantified to values ranging from ~0 to 40%.

Rock samples from the exploratory wells A, B, C and D were crushed at < 80 μm before analysis with X-ray diffraction (XRD), scanning electron microscopy (SEM), transmission electron microscopy (TEM), and energy dispersive X-ray spectroscopy (EDX). Magnetic separations were performed on some samples and the magnetic fractions were analyzed with the techniques aforementioned. XRD was performed with a Bruker D5000 or D8 diffractometer using CuKα radiation. The instruments were operated with a step size of 0.026° 2θ and a counting time of 8 s. The divergence slit, anti-scatter slit, and detector slit were 0.6, 0.6, and 0.2 mm, respectively. SEM was performed on a Zeiss Ultra 55 FEG microscope operated at 10 kV and a working distance of 7.5 mm using mostly a backscatter detector for imaging. This SEM is equipped with an energy dispersive X-ray system from Bruker. TEM was performed on a Jeol FEG 2100F operated at 200 kV equipped with an energy dispersive X-ray system from Jeol.

The amount of magnetite in rock samples was estimated from the measurement of the saturation magnetization Js (Malvoisin *et al.*, 2012), which is directly proportional to the quantity of magnetite. Rock samples were firmly packed in non-magnetic capsules which were placed in a Princeton Micromag Vibrating Sample Magnetometer 3900 for magnetization measurements. A proportionality factor of 92 $Am^2 \cdot kg^{-1}$ was used to convert the Js values (saturation magnetization) into a quantity of magnetite (Malvoisin *et al.*, 2012).

The total iron content and the Fe^{2+} content of rock samples were determined at the CNRS Service d'Analyse des Minéraux et des Roches in Nancy, France. The analytical

procedure for total iron was described by Carignan *et al.* (2001) for trace elements. The rock samples are decomposed using alkali fusion and analyses are done by flow injection ICP OES Icap 6500 from Thermo with a radial flame. For analysis of the Fe^{2+} content, the rock sample is dissolved by hot acid etching with hydrofluoric and sulfuric acid for ~10 min. The sample is then cooled at ambient temperature and the Fe^{2+} is quantified by volumetric analysis using potassium dichromate in the presence of boric and phosphoric acid.

Gas chromatography attached to a mass spectrometer was used to measure carbon isotopic composition of the carbonate fraction in the rock samples from the Famenian diamictite of Well A, B and C. The protocol used was the one described by Lebeau *et al.* (2014). Combined in the same sample, siderite and calcite were able to be measured separately because of their different responses to acidification. In a tube under helium atmosphere, the rock samples, as powders < 80 μm, were first acidified with pure H_3PO_4 for 4 h at ambient temperature: the calcite $CaCO_3$ was wholly destabilized. The headspace of the tube, made of helium and CO_2 from calcite, was then analyzed. The tube was flushed a second time with helium, and heated at 120°C for 2 h: the siderite $FeCO_3$ was destabilized and the headspace was analyzed. Lebeau *et al.* (2014) showed that the organic matter does not destabilize during this protocol, and thereby does not disturb the CO_2 signal from the carbonates. The uncertainty in $\delta^{13}C$ of carbonate is ± 0.1‰.

The Rock-Eval methodology

The methodology described by Pillot *et al.* (2014) to characterize and quantify the carbonates in rock samples using the Rock-Eval instrument has been adapted for our samples, which contain small amounts of siderite together with highly mature organic matter. This analytical work represents one of the first applications of the method developed by Pillot *et al.* on natural rock samples.

The Rock-Eval instrument has been mainly designed to study the quality of organic matter and the petroleum potential of source rocks. Pillot *et al.* (2014) showed that it allows also for the characterization and quantification of the different types of carbonates. Because each carbonate has its own temperature of decomposition (T_{max}), and because only CO_2 is released from decomposition of carbonates, it is possible to identify and quantify the carbonates present in a sample using the Rock-Eval oxidation cycle. For siderite which is destabilized at a temperature of ~500°C, the CO_2 signal can be disturbed by the destabilization of organic matter (Fig. 3a). Unlike carbonates, organic matter emits CO in addition to CO_2 and the CO/CO_2 ratio of the organic matter was found relatively constant along the temperature ramp (Fig. 3a). Using the CO signal, the CO_2 linked to the decomposition of organic matter could be estimated and removed from the total CO_2 signal, allowing the calculation of the CO_2 released from carbonates (Fig. 3a).

When carbonates are the dominant source of CO_2 or when destabilization temperatures between carbonates and organic matter are substantially different, as is the case for calcite or dolomite, the CO_2 signal of the carbonates can be easily corrected for organic matter. In our study, the aim was to quantify amounts of siderite, with a T_{max} lower than that of calcite and dolomite and close to the T_{max} of organic matter oxidation. Also, the siderite proportion could be in some samples smaller than the amount of organic matter. Under such conditions, we used the pyrolysis cycle rather than the oxidation cycle. The maximum temperature of 650°C reached by the pyrolysis oven is sufficient to destabilize the siderite, although not enough for calcite and dolomite. Due to the high maturity of the source rock of the Solimões basin, the CO_2 released by the organic matter during pyrolysis was negligible, which was indicated by the low amount of released CO (Fig. 3b). Thus, the CO_2 signal from the siderite was no longer disturbed by the destabilization of the organic matter.

In reducing conditions, the destabilization of the iron carbonate produced some CO associated with CO_2 according to the reaction:

$$2FeO + CO_2 = Fe_2O_3 + CO \quad (3)$$

The produced CO represents less than 2% of the released CO_2. The error, therefore, associated with the siderite quantification during pyrolysis due to the emission of CO is much lower than the error due to the siderite-organic matter interference when using an oxidation cycle. Quantification of other carbonates (mainly calcite) was obtained by a post-pyrolysis oxidation cycle. Tests were performed to validate the efficiency of the Rock-Eval methodology for the quantification of carbonates regarding the Solimões samples (see Appendix A).Based on the calibration curve for pure siderite, the uncertainty on the siderite quantification is of ±5% and the detection limit of siderite in the Solimões samples was of ~0.02wt.%.

4. RESULTS

4.1 Gas and water samples

The gas accumulations in the Solimões basin are largely made of hydrocarbons, especially methane, which can represent up to 95 mol.% of the gas (Table 1). N_2 is also present, ranging from 1 to 25 mol.% and the CO_2 content is ~0.2 mol.%. H_2 was mostly detected in traces but it reaches occasionally high concentrations up to 6 mol.% (Table 1). The maturity of the hydrocarbon gases increases from the east to the west, with values of the C_2/C_3 ratio ranging from 2 to 16 (Table 1, Fig. 4a), which corresponds to maturities from the end of the oil window to extreme secondary cracking (e.g., Prinzhofer and Huc, 1995). The distribution of wells A, B, C and D follows basically an east-west trend, with an increase of the gas maturity from Well A to D.

The isotopic composition of the Solimões gases is given in Table 1 and plotted as a function of the carbon numbers in the hydrocarbons (Fig. 4b). Carbon isotopic patterns ($\delta^{13}C$) of alkanes containing from one to four carbon atoms (C_1 to C_4) show basically two main isotopic trends. In the eastern part of the basin where gas maturity is relatively low (i.e., Well A, B, H and I) (Fig. 4a), gas samples show $\delta^{13}C$ decreasing with the number of carbon atoms and values of $\delta^{13}C_1$ ranging from ~-35‰ to -41‰. This corresponds to a usual isotopic signature, typical of a thermal generation (Des Marais *et al.*, 1981). In hydrocarbon gases of high maturity in the west of the basin (i.e., Well C, G and F) (Fig. 4a), the $\delta^{13}C$ of methane is heavier with values reaching ~-30‰, and complete reversals of the normal trends of carbon isotopic composition are observed, i.e., $\delta^{13}C_1 > \delta^{13}C_2 > \delta^{13}C_3 > \delta^{13}C_4$.

The iron and calcium concentrations of the formation waters of the Solimões basin, after correction from the contamination by drilling mud, are given in Table 2 and compared to the values of brines from the Central Mississippi Salt Dome basin (Kharaka *et al.*, 1987), which are considered as good representatives of metal-rich brines that formed ore deposits in sedimentary rocks worldwide (Fig. 5). The iron concentrations of the Solimões waters reach values up to 1000 $mg \cdot L^{-1}$, in the same range of concentration as the highest values measured by Kharaka *et al.* (1987). These iron concentrations likely represent a minimum as oxidation during the sampling process may have led to partial precipitation of dissolved iron. The Ca^{2+} concentrations are also comparable to those of the Mississippi basin.

The temperature measured in the source rock of the basin is ~100°C (temperature logging) and the lithostatic pressure is estimated to be ~30 MPa. Under these conditions, the CO_2 content of 0.2 mol.% measured in the Solimões gases corresponds to a CO_2 activity in water of ~5 *m*molal. The Fe^{2+} and Ca^{2+} concentrations at equilibrium with siderite and calcite, respectively, are calculated at 100°C and 30 MPa according to the reaction

$$MCO_3 + 2H^+ = M^{2+} + CO_{2,aq} + H_2O \quad (4)$$

where M^{2+} is a divalent cation, iron or calcium in this case. For pH values between 4.5 and 5.5, i.e., the range of pH values measured by Kharaka et al. (1987) in the Mississippi basin, the Fe^{2+} and Ca^{2+} concentrations range from 10 to 1000 mg·L^{-1} and 2000 to 200 000 mg·L^{-1}, respectively. The Fe^{2+} and Ca^{2+} concentrations measured in the Solimões brines are consistent with these ranges of concentrations (Table 2, Fig. 5). Assuming a pH similar to that of the Mississippi brines, the analyzed fluids might be close to equilibrium with siderite and calcite.

4.2 Rock samples

4.2.1 Siderite, calcite and magnetite content

No siderite was detected in the reservoir rocks of the Solimões basin (Fig. 6a). The siderite content increases in the Famenian diamictite reaching up to 7 wt.% of the rock in Well A, and then decreases in the same well in the Frasnian shale. The siderite content in the Famenian diamictite is not homogenous. Samples containing > 4 wt.% of siderite are frequently observed in Well A, whereas in Well B and C, the siderite contents reach maximal amounts of ~2.5 and ~0.5 wt.%, respectively. In the Famenian diamictite of Well D, no siderite was detected. The iron carbonate content evolves according to an east-west trend, with a decrease of the siderite content as the maturity of the hydrocarbon gases increases (Fig. 4a).

The calcite content decreases basically from the Carboniferous reservoir rocks to the Devonian source rocks to reach values mostly lower than 3 wt.% (Fig. 6b). In addition to this global tendency, Well D, free of siderite, shows a local increase in the amount of calcite in the

Famenian diamictite, whereas in Well A, B and C in which siderite was detected, the calcite content remains low (Fig. 6b).

SEM observations of rock samples from the Famenian diamictite of exploratory wells A, C and D are shown in Fig. 7. In Well A, the surface of siderite is clean without observable etch pits nor irregularities. The EDX pattern indicates low amounts of Mg and Ca (Fig. 7), but the chemical composition is close to the iron end-member. In contrast to Well A, siderite from Well C exhibits an altered surface with dissolution pits. In Well D, consistent with the Rock-Eval analyses, no siderite was detected; instead, a fibrous mineral phase was observed together with small and light grains. The EDX pattern of these grains indicated a composition of primarily iron and oxygen (Fig. 7), consistent with iron oxide. This was confirmed by the x-ray diffraction patterns which indicated the presence of Fe-rich silicate and magnetite.

Relatively low amounts of magnetite were detected in the Famenian diamictite compared to the amounts of siderite (Fig. 8a). In Well A and B, the magnetite content is of 0.1 wt.% whereas up to 7 wt.% of the rock is made of siderite. The magnetite content increases to 0.2 wt.% in Well D in which no siderite was observed. No magnetite was detected in the Famenian diamictite of Well C; however, SEM and EDX analysis indicated the presence of pyrite (FeS_2), which was not observed in the other wells (Fig. 8b). The occurrence of pyrite rather than magnetite suggests that different processes occurred, likely related to more reducing conditions.

4.2.2 Total iron content

The total iron content from the Carboniferous reservoir to the Frasnian shale in Well A to D follows basically the same trend as the siderite content (Fig. 9a). Apart from Well D, the iron content is relatively low in the Carboniferous reservoir and increases in the Famenian

diamictite to reach up to 4 wt.% of the rock in Well A. As for siderite, the iron content decreases from Well A to D, suggesting that the siderite content governed iron content. In Well D in which no siderite is present, the iron content still represents 2 wt.% of the rock, supporting the presence of Fe-bearing minerals other than siderite. In the Frasnian shale, apart from Well C, the evolution of iron content from Well A to D is reversed compared to the Famenian diamictite. The iron content is the highest in samples of Well D and decreases toward the east of the basin, i.e., in Well B and A. The especially low amounts of iron in the Frasnian shale of Well C confirmed that different processes occurred in this well, which was already evidenced by the occurrence of pyrite in the Famenian diamictite (Fig. 8b). The evolution of total iron content is associated with a change of iron speciation (Fig. 9b). The percentage of ferric iron increases from the Famenian diamictite to the Frasnian shale to reach up to 35% of the total iron. Such evolution of the iron speciation was relatively unexpected considering the marine origin of the Frasnian shale, which suggests a more reducing depositional environment than that of the Famenian diamictite periglacial formations.

The total iron and siderite content in the Famenian shale allows the calculation of the distribution of iron between siderite and other mineral phases (Fig. 10a). The decrease of the total iron content from Well A to D is due only to the decrease of siderite. Concurrently, the amount of iron carried by mineral phases other than siderite remained constant from Well A to Well D, in which all the iron is carried by other mineral phases. TEM observations and electron diffraction patterns of samples of the Famenian diamictite of Well D indicate the occurrence of olivine (Fig. 10b). The XRD patterns confirmed the occurrence of olivine and pyroxene, which likely account for the background of iron (Fig. 10a). In addition, minerals showing tubular structures typical of serpentines were observed (Fig. 10c).

4.3 Carbon isotopic composition of siderite and calcite

The carbon isotopic compositions of siderite and calcite from samples of the Famenian diamictite of Well A, B and C are given in Table 3. The $\delta^{13}C$ of siderite is plotted against that of calcite (Fig. 11). The carbon isotopic composition of the iron carbonates range from -5‰ to -13‰, while the $\delta^{13}C$ of the calcite is heavier with values between -6‰ to 3‰. The isotopic composition of the siderite is consistent with a diagenetic origin, i.e., a source mixing carbon from organic matter with $\delta^{13}C$ lower than -20‰ and dissolved inorganic carbon with $\delta^{13}C$ value of ~0‰ (e.g., Schidlowski, 2001). The heavier $\delta^{13}C$ of calcite suggests a marine origin.

5. DISCUSSION

5.1 Thermodynamic calculations

Equilibrium constants were calculated with the SUPCRT92 package (Johnson *et al.*, 1992) which incorporates thermodynamic data from Helgeson *et al.* (1978) for minerals, and Shock and Helgeson (1988) and Shock *et al.* (1989, 1997) for dissolved inorganic aqueous species. The stability domain of a poorly ordered carbonaceous material used as a proxy for kerogen (referred in Fig. 12b as Carbo. mat.) was calculated by assuming that this phase has thermodynamic properties similar to those of graphite at temperature of ~200°C, which is consistent with the experimental results of Milesi *et al.* (2015). The equilibrium constants K_s from the dissolution reactions of calcite, magnesite and siderite (Reaction 4) are calculated as a function of temperature (Fig. 12a). The three carbonates have a retrograde solubility meaning that the constants K_s decrease with increasing temperature. Thus, for a fluid composition at equilibrium with calcite or magnesite, an increase in temperature promotes the precipitation of the two carbonates. In the case of siderite, the fluid composition must also satisfy appropriate redox conditions. If the temperature increases from 100 to 200°C, a fluid

composition at hypothetical equilibrium with siderite, magnetite and carbonaceous material at 100°C becomes oversaturated relative to Fe^{3+}-bearing iron oxide, and undersaturated relative to siderite (Fig. 12b). Consequently, siderite dissolves and releases CO_2. Part of the released ferrous iron oxidizes and produces Fe^{3+}-bearing minerals such as magnetite and some H_2 through H_2O reduction according to Reaction (2) (McCollom, 2003).

Milesi *et al.* (2015) have shown experimentally that the dissolution of siderite at 200 - 300°C and 50 MPa in a closed system produces magnetite and carbonaceous material along with residual siderite. In addition, the H_2 and CO_2 compositions of the fluid were measured close to equilibrium with the siderite – magnetite – graphite mineral assemblage. Considering a closed system, the evolution of the fluid composition after a rapid increase in temperature from 100 to 200°C is calculated taking into consideration an initial and final fluid composition equal to the H_2–CO_2 composition at hypothetical equilibrium with siderite, magnetite and carbonaceous material at 100 and 200°C, respectively (Fig. 12b). Firstly, siderite dissolves until the attainment of equilibrium with the siderite – magnetite mineral assemblage according to the reaction

$$3\ FeCO_3 + H_2O = Fe_3O_4 + 3\ CO_2 + H_2 \quad (5)$$

Then, the fluid composition evolves toward equilibrium with carbonaceous material according to:

$$CO_2 + 2H_2 = C + 2H_2O \quad (6)$$

This two-steps reaction path is supported by the laboratory hydrothermal dissolution experiments of siderite by Milesi *et al.* (2015), in which it is shown that the fluid composition equilibrates relatively rapidly with siderite and magnetite through Reaction (5) whereas Reaction (6) is more sluggish. Considering a porosity of ~15% saturated with water, and a thickness of ~30 m for the Famenian diamictite, the amount of siderite consumed along the

compositional path described in Fig. 12b is ~78 $kg \cdot m^{-2}$. The average content of siderite in the eastern part of the basin is ~4 wt.% (Fig. 6a), i.e. ~3400 $kg \cdot m^{-2}$, meaning that only ~2 wt.% of siderite would dissolve in response to a temperature increase from 100 to 200°C in the Famenian formation. This calculation is performed for a closed system, where all the generated and solubilized compounds continue to interact in the system. Any opening of the system associated with the release of fluids would result in an increase in the proportion of the solubilized siderite. From Well A to Well D, the measured decrease of the siderite content is of ~100% (Fig. 6a), i.e., two orders of magnitude higher than the extent of dissolution calculated considering a closed system.

5.2 Unconventional generation of CH_4 from siderite

The detection of siderite in the Famenian diamictite of the Solimões basin (Fig. 6 and 7) is consistent with the especially high concentrations of iron measured in the formation waters (Table 2, Fig. 5). The siderite content was found to decrease from up to 7 wt.% in the eastern part of the basin (Well A) to less than 0.02 wt.% in western part (Well D) (Fig. 6). Changes in the depositional conditions of the Famenian formation could explain the decrease of siderite. Indeed, an increase of the oxidative conditions toward west during deposition of the Famenian formation would render the siderite unstable; however, it is not consistent with the relatively constant content of organic matter from Well A to D (Fig. 2b). The decrease of the total iron content which occurs concurrently with the decrease of siderite rather suggests a gradual alteration of the iron carbonate in an open system. During the Triassic, a magmatic event led to the development of two dolerite sills in the eastern part of the basin and three dolerite sills in the western part, with the third lower sill being located very close to the Devonian source rock (Fig. 1b). Elias *et al.* (2007) measured the $\delta^{18}O$ values of dolomite from

the Carboniferous reservoir rocks and calculated the precipitation temperatures of the carbonate. Their study area was located to the east of Well A where the diabase intrusions are relatively distant from the petroleum system (Fig. 1b). The authors reported a precipitation temperature up to 155°C; higher precipitation-temperatures can be expected toward west. The increase of thermal stress from Well A to Well D likely led to hydrothermal activities associated with the Devonian source rock, resulting in the dissolution of siderite. The SEM observation of etch pits on the surface of siderite from Well C in the area affected by the three dolerite sills is consistent with this scenario (Fig. 7). The same kind of dissolution images were observed by Milesi *et al.* (2015) on the surface of siderite reacted in hydrothermal experiments.

Following the increase in temperature, the fluid becomes undersaturated relative to siderite which undergoes an oxidative dissolution releasing CO_2 and producing H_2 through a redox reaction between H_2O and Fe^{2+} (Fig. 12b) (McCollom, 2003; Milesi *et al.*, 2015). That is, iron oxide and especially magnetite could have formed through the partial oxidation of Fe^{2+} into Fe^{3+}. In the Famenian diamictite, the amount of magnetite increases by a factor ~2 from the east to the west of the basin; however, this magnetite content cannot account for all of the oxidation of the iron from the siderite in the western part of the basin because the magnetite content in Well D is ~one order of magnitude lower than the siderite content in Well A (Fig. 8). Apart from Well C, the total amount of iron in the Frasnian shale increases as it decreases in the Famenian diamictite (Fig. 9a). In addition, the percentage of Fe^{3+} increases from the top to the bottom of the Devonian source rocks (Fig. 9b), which is inconsistent with the marine and terrestrial origin of the Frasnian and Famenian formation, respectively. One explanation is that iron, released from siderite in the Famenian diamictite, migrated in the Frasnian shale. The migration of iron is supported by the calculations which show that, considering a closed system, only ~2 wt.% of siderite would have been consumed to

reequilibrate the fluid with the siderite – magnetite – carbonaceous material assemblage in response to an increase of temperature from 100 to 200°C (Fig. 12b). Instead, from Well A to D, the siderite content decreases from ~7 to 0 wt.%, meaning complete dissolution of siderite, which can only be achieved in an open system. This scenario is also consistent with the location of the diabase intrusions that likely induced fluid circulation from the top to the bottom of the Devonian source rocks.

The significant amounts of H_2 in some samples are consistent with the oxidative dissolution of siderite; however, in most samples, H_2 is present as traces (Table 1). The east-west decrease of the siderite content is correlated with an increase of the gas maturity and an increase of the $\delta^{13}C$ of methane (Fig. 4). Experiments of siderite decomposition at 200 to 300°C produced CH_4 and other reduced carbon compounds such as polycyclic aromatic hydrocarbons from reaction between CO_2 released from siderite and H_2 (McCollom, 2003; Milesi *et al*,. 2015). The reaction of production of CH_4 from CO_2 reduction can be written as

$$CO_2 + 4H_2 = CH_4 + 2H_2O \quad (7)$$

With values of its equilibrium constant at 50 MPa, 200 and 300°C of $10^{17.5}$ and $10^{11.4}$, respectively, Reaction (7) is highly favored in the direction of CH_4 generation. In addition, Milesi *et al.* (2015) have shown experimentally that the fluid generated by the siderite dissolution tends to equilibrate with the siderite – magnetite – graphite mineral assemblage, which corresponds to relatively high CO_2 and H_2 concentrations favorable for CH_4 generation. Such generation of CH_4 in the Solimões basin is consistent with the inverse correlation observed between the siderite content and the gas maturity. Moreover, CH_4 produced from siderite can be expected to be enriched in heavy ^{13}C vs ^{12}C because of the heavy $\delta^{13}C$ of the carbon source. Indeed, the carbon isotopic composition of siderite from the Famenian diamictite was measured between -5 and -13‰ (Fig. 11). Thus, in addition to the increase in

gas maturity, formation of CH_4 from siderite is consistent with the high $\delta^{13}C_1$ measured in the western part of the basin (Fig. 4). On the other hand, hydrogenation of the residual kerogen hosted in the Famenian diamictite may also offer another source of carbon for the formation of ^{13}C-rich methane according to:

$$C_{(s)} + 2H_2 = CH_4 \quad (8)$$

It is known that thermogenic hydrocarbons of high maturity can also produce methane with heavy $\delta^{13}C$ (e.g., Clayton, 1990). This might have occurred in the western part of the Solimões basin but all the evidence previously shown of siderite reactivity and of its correlation with gas maturity suggests that reactions (7) and/or (8) contributed to the gas budget in the basin. It can be noted that, according to reactions (7) and (8), the building up of high H_2 concentrations is feasible in case of low CO_2 activities or of low reactivity of the kerogen; otherwise, the equilibria suggest the production of large amounts of CH_4. This seems consistent with the observations of H_2-rich fluids in carbon-depleted environments such as siliceous shields (e.g., Newell *et al.*, 2007; Larin *et al.*, 2014), ophiolitic contexts (e.g., Abrajano *et al.*, 1988; Hosgormez *et al.*, 2008) or old sediments with low amounts of organic matter and carbonates; while sedimentary basins rich in organic matter and carbonates such as the Solimões basin host large amounts of hydrocarbon gases but are mostly free of H_2.

In the western part of the basin, the hydrocarbon gases showed partial or complete reversals of the "normal" carbon isotopic trends (Fig. 4). Dai *et al.* (2004, 2008) proposed that mixing between thermogenic and abiotic hydrocarbon gases could account for reversals of the carbon isotopic compositions. The isotopic inversion observed between the C_1 and C_{2+} compounds (Fig. 4b) associated with the high maturity gas and the heavy $\delta^{13}C$ of methane in the western part of the Solimões basin could support the occurrence of Fischer-Tropsch-Type reactions. Iron oxides produced from siderite dissolution could act as surface catalyst for

abiotic CO_2 reduction and polymerization (e.g., Foustoukos and Seyfried, 2004; Fu *et al.*, 2007; Milesi *et al.*, 2015). The complete isotopic reversal from C_1 to C_3 observed in the western part of the basin suggests a low content of thermogenic ethane and propane, which is consistent with the high maturity of the gases (> 90 mol.% of methane, Table 1) resulting from a severe secondary cracking induced by the diabase intrusions (Eiras, 1998a).

As mentioned in the introductory part of this work, other processes can lead to isotopic anomalies and some of them may have occurred concurrently to the production of CH_4 derived from the decomposition of siderite. Burruss and Laughrey (2010) proposed that, at temperatures higher than 200°C, ethane and propane can react with water and redox active transition metals to produce CH_4 and reversals in the isotopic composition of alkanes. This process was proposed, in addition to mixing, to explain complete reversal from methane to propane in the gas reservoir of the northern Appalachian basin. Mixing between gases of different maturities was proposed to explain reversals of the carbon isotopic composition in natural gas (e.g., Jenden *et al.*, 1993). In the Solimões basin, a mixing between a low-maturity gas in the eastern part of the basin and a gas of higher maturity in the western part could explain the occurrence of the observed isotopic anomalies together with the production of CH_4 related to siderite decomposition. But this mixing mechanism, which might well have occurred to some extent, fails to explain the correlation observed between gas maturity and the mineralogical evolution of siderite. Two other mechanisms are known for their ability to build up such geochemical anomalies: thermochemical sulfate reduction (Krouse *et al.*, 1988) and microbial oxidation of methane (James and Burns, 1984). However, they also fail to explain the siderite-maturity observed correlation and they cannot produce the full pattern observed. Indeed, Krouse et al. (1988) suggested that ethane and propane are preferentially affected by thermochemical sulfate reduction which thus induces an increase of the $\delta^{13}C_2$ and $\delta^{13}C_3$ as the sulfate reduction increases, and microbial activity was proposed to affect

preferentially propane, n-butane and n-pentane, resulting in partial reversals of the carbon isotopic composition of natural gases (e.g., Katz, 2011).

5.3 Qualitative approach of H_2, CH_4 and CO_2 generation

5.3.1 Siderite mass balance

Consistent with the experimental study by Milesi *et al.* (2015) and with the mineralogical evolution of siderite observed in the Solimões basin (Fig. 7), Reaction (5) is used to estimate the yield of CO_2 and H_2 resulting from the dissolution of siderite in the Solimões basin. The relatively constant amounts of organic matter from Well A to Well D suggests relatively constant depositional conditions of the Famenian formation (Fig. 2). Thus, the siderite content on the east of the basin is considered representative of the initial content of siderite in the whole basin before the magmatic intrusions. Considering an initial average content of siderite in the Famenian diamictite of ~4 wt.% (Fig. 6), ~220 and 650 $m^3 \cdot m^{-2}$ of H_2 and CO_2, respectively, would be produced from the complete dissolution of siderite. The H_2 generation could even be about 50% higher if ferrous iron from the siderite was entirely oxidized by reaction with water rather than being partly preserved into magnetite. The entire consumption of H_2 to produce CH_4 is consistent with molecular hydrogen being present mostly as traces in the gas accumulation of the Solimões basin. Considering reactions (7) and (8), the maximal amounts of methane deriving from the decomposition of siderite range between 50 and 110 $m^3 \cdot m^{-2}$.

Considering Reaction (7), a maximal amount of ~8% of CO_2 released from siderite would convert into CH_4, which is not consistent with the low CO_2 content of ~0.2 mol.% observed in the gas accumulations of the Solimões basin. Other processes such as carbonate precipitation may explain the depletion of CO_2. Unlike siderite, precipitation of calcite or

magnesite is favored by an increase in the thermal stress (Fig. 12a). In the Famenian diamictite of Well D in which siderite dissolved completely, the calcite content increases up to ~10 wt.% while it remains at lower values in the eastern wells less affected by siderite dissolution (Fig. 6). The precipitation of calcite is also consistent with the high concentrations of Ca^{2+} measured in the formation water (Table 2, Fig. 5). Additionally, in terms of CO_2 mass balance, the amount of siderite measured in the eastern part of the Famenian diamictite (Well A) is consistent with the calcite content in the western part (Well D).

The magnitude of unconventional methane generation of ~110 $m^3 \cdot m^{-2}$ is compared to the yield of CH_4 from the usual thermal cracking of organic matter. The total organic carbon content in the Famenian diamictite is of ~1 wt.% (Fig. 2), and the yield of hydrocarbon generation from the TOC was estimated at 50%. Considering that 60% of this hydrocarbon generation affect only methane generation (including primary and secondary cracking), the production of thermogenic CH_4 from the Famenian diamictite is estimated around 470 $m^3 \cdot m^{-2}$. As a result, siderite-derived CH_4 could represent up to ~ 20% of the total CH_4 produced by the Famenian diamictite. If an uncertainty of 1 wt.% is considered on the initial average content of siderite, the maximal contribution of the siderite-derived CH_4 would range from 15 to 22% of the total CH_4.

5.3.2 Isotopic approach

An estimation of the amounts of unconventional CH_4 produced from siderite could also be achieved based on the isotopic data. However, although widely discussed in the literature, the isotopic fractionations resulting from the reduction of CO_2 or CO into CH_4 remain poorly constrained (McCollom, 2013), such that only a broad estimation of the CH_4 deriving from the siderite decomposition can be obtained from the isotopic data.

In the western part of the Solimões basin, the absence of siderite indicates that iron carbonate likely decomposed entirely into CO_2, resulting in no isotopic fractionation between CO_2 and siderite because of the total reaction yield. In hydrothermal experiments of Fischer-Tropsch-Type synthesis with CO_2-H_2 rich fluids in the presence of mineral catalysts, Horita and Berndt (1999), McCollom and Seewald (2006) and McCollom *et al.* (2010) reported production of CH_4 showing isotopic fractionation of ~-30‰ with the carbon source ($\varepsilon_{CH4\text{-}source}$). Similar isotopic fractionation between CO_2 and CH_4 were proposed by Proskurowski *et al.* (2008) in fluids venting from the hydrothermal systems of Lost City. As the highest $\delta^{13}C$ for siderite in the Solimões basin is ~-5‰ (Table 3, Fig. 11), an isotopic fractionation of ~-30‰ between CO_2 and CH_4 would result in $\delta^{13}C_1$ values of ~-35‰, which cannot account for the values up to ~-30‰ measured in the western part of the study area (Fig. 4).

In experiments involving CO_2-H_2 bearing fluids and magnetite at 400°C, Fu *et al.*, (2007) determined CH_4-CO_2 isotopic fractionation of ~-15 to -20‰, which is consistent with the values of $\varepsilon_{CH4\text{-}source}$ reported by Hu *et al.* (1998) and Taran *et al.* (2007) in Fischer-Tropsch-Type experiments. Considering this CH_4-CO_2 isotopic fractionation and a $\delta^{13}C$ value for siderite of ~-5‰ (Table 3, Fig. 11), the siderite-derived CH_4 would have a $\delta^{13}C$ of ~-20‰. Due to the high thermal maturity of hydrocarbon gases in the western part of the basin, the thermogenic methane can be expected to be relatively enriched in ^{13}C relative to ^{12}C (e.g., Clayton 1990). For the calculation, we considered a $\delta^{13}C$ value of thermogenic methane to the west of -34‰, i.e., the highest value of $\delta^{13}C_1$ measured in the eastern part of the basin (Fig. 4). Therefore, the value of $\delta^{13}C_1$ of up to ~-30‰ measured in the western part of the basin (Fig. 4) could be explained by a gas mixing between 80 mol.%. of thermogenic CH_4 with a $\delta^{13}C$ of ~-34‰ and 20 mol.% of siderite-derived CH_4 with a $\delta^{13}C$ of ~-20‰. This calculation is subject to significant uncertainties as both the values of $\varepsilon_{CH4\text{-}CO2}$ and of the thermogenic endmember of $\delta^{13}C_1$ in the west part of the basin are poorly constrained. As an example, if a

value of $\varepsilon_{CH4\text{-}CO2}$ of -25‰ is considered, i.e., close to the values measured in the laboratory experiments of McCollom and Seewald (2006), the siderite-derived CH_4 would have a $\delta^{13}C$ of ~-30‰. In that case, the isotopic signature of the methane in the west part of the basin would be fully explained by the siderite-derived CH_4, which is not consistent with the siderite mass balance. Similarly, considering a thermogenic endmember of $\delta^{13}C_1$ in the west part of the basin of ~-40‰ instead of -34‰ and a $\delta^{13}C$ of siderite-derived CH_4 of ~-20‰, the contribution of the siderite-derived CH_4 would be of 50%. Thus, based on the isotopic data, the contribution of the hydrothermal decomposition of siderite to the gas budget is poorly constrained; however, a contribution of 20% is calculated when conservative input parameters are considered, which is consistent with the calculations based on the siderite mass balance (see section 5.3.1).

5.4 The origin of siderite

The detection of primary silicates such as olivine and pyroxene in the source rock of the Solimões basin was unexpected as these minerals are the least stable under the present temperature and pressure conditions (Bowen's reaction series) (Fig. 10b). One possible explanation for the occurrence of olivine and pyroxene in the Famenian formation is the physical alteration of basic to ultrabasic crystalline basement producing detrital particles incorporated in the periglacial formation during the early stage of diagenesis. Electron microscopy of tubular microstructures typical of serpentinites (Fig. 10c) indicates that olivine and pyroxene started to undergo aqueous alteration. During early diagenesis prior to the magmatic events, the release of CO_2 from the thermal maturation of organic matter combined with the alteration of the Fe-rich primary silicates may have produced conditions favorable for siderite precipitation. Alteration experiments of basic and ultrabasic rocks with fluids rich in

dissolved inorganic carbon (DIC) showed the precipitation of siderite or Fe-rich magnesite (Jones *et al.*, 2010; Saldi *et al.*, 2013). These experimental results together with the observed coexistence of olivine and siderite in the Solimões basin suggest that siderite may have resulted from aqueous alteration of primary silicates during diagenesis prior to the magmatic events.

The persistence of primary silicates in the source rocks indicates that they resisted the alteration potentially induced by the diabase intrusions. Studies of olivine carbonation at relatively low temperatures down to ~90°C with CO_2-saturated water showed the formation of silica layers at the surface of olivine (e.g., Daval *et al.*, 2011; Sissmann *et al.*, 2013). The authors proposed that such silica coating constitutes a barrier for the transport of aqueous species and inhibits the dissolution of olivine. In the Solimões basin a similar mechanism may have preserved basic and ultrabasic minerals from complete alteration. This is consistent with the observation of a constant content of Fe-bearing minerals other than siderite, regardless of the proximity to the diabase intrusions (Fig. 10a). The persistence of the primary silicates regardless of the increase of the thermal effect also disproves them as being the main source of H_2. To the contrary, siderite did not resist the increase of the thermal stress and dissolved to produce ferric iron and H_2 (McCollom, 2003; Milesi *et al.*, 2015). In the Solimões basin, siderite could represent an intermediate in the production of reducing conditions from the alteration of ultrabasic and basic minerals.

Alternatively, it cannot be ruled out that the observed olivine and pyroxene can be contaminants from the upper diabase intrusions mixed into cutting samples from the source rocks during the drilling. Other sources of iron would then be necessary for siderite to form during diagenesis, which is consistent with the elevated iron concentrations measured in the brines (Fig. 5). Finally, siderite could have been inherited from the deposits of the periglacial formation, i.e., the Famenian diamictite.

In these three cases, a diagenetic origin of siderite is supported by the carbon isotopic values between -5 and -13‰ (Table 3, Fig. 11), which suggest that the carbon source of the siderite likely results from a mixing between DIC from sea water with a $\delta^{13}C$ of ~0‰ and CO_2 from organic matter with a $\delta^{13}C$ of less than ~-20‰ (e.g., Schidlowski, 2001).

6. CONCLUSION

Siderite in the Solimões basin has played a primary role through the setting of highly reducing conditions at the origin of unconventional generation of CH_4. The increased thermal stress in the western part of the basin induced partial to complete oxidative dissolution of the siderite hosted in the Famenian diamictite. During the thermal maximum, a redox reaction between water and siderite-derived Fe^{2+} produced H_2 consistent with the experimental studies of McCollom (2003) and Milesi *et al.* (2015). The correlation between the decrease in siderite content and the increase in gas maturity and isotopic anomalies is consistent with the reaction between H_2 and a carbon source, CO_2 or kerogen, to produce CH_4. Such unconventional generation of CH_4 is close to the process forming light hydrocarbons in ultrabasic contexts, in which H_2 is derived from the hydrothermal alteration of olivine and pyroxene. These minerals were also observed in the source rock of the Solimões basin; however, the absence of a correlation between their constant content and the increasing gas maturity leads us to propose that they were not directly involved in H_2 generation, but rather acted as a source of iron, direct or indirect, for siderite precipitation during diagenesis. Whatever the origin of siderite, independent quantitative approaches based on siderite mass balance and isotopic data indicate that ~20% of the accumulated CH_4 in the western part of the Solimões basin resulted from the oxidative dissolution of siderite. The generation of hydrocarbon gases deriving from hydrothermal decomposition of siderite with economic significance may be widespread in

petroleum basins which underwent high thermal stress. The level of thermal stress required for this mechanism to have significance on the gas budget in petroleum basins still needs to be assessed.

Acknowledgements

This work was financially supported by the Institut de Physique du Globe de Paris, the HRT Oil and Gas company and the IPEXCo company. The transmission electron microscopy facility at IMPMC was purchased by Region Ile de France Grant SESAME 2000 E 1435. The authors are grateful to Barry J. Katz, Robert C. Burruss and an anonymous reviewer for greatly improving the manuscript. We are also grateful to all members of the analytical laboratories of the IPEXCo company and especially to Caroline Magnier for the sample selection and preparation. We appreciate stimulating discussions with the scientific members of the HRT Oil and Gas company and with the members of the Department of Stratigraphy and Paleontology at the University of State of Rio de Janeiro. We are sincerely thankful to Egberto Perreira and Carmen Alferes for their technical support for the Rock-Eval analyses, and to Julie Carlut who carried out the magnetization measurements at the Institut de Physique du Globe de Paris.

REFERENCES

Abrajano T. A., Sturchio N. C., Bohlke J. K., Lyon G. L., Poreda R. J. and Stevens C. M. (1988) Methane-hydrogen gas seeps, Zambales Ophiolite, Philippines: Deep or shallow origin? *Chem. Geol.* **71**(1), 211-222.

Bender A. A., Eiras J. F., Wanderley Filho J. R. and Barbosa Filho C. M. (2001) Quantificação 3D da evolução termal da Bacia do Solimões e suas implicações petrolíferas. *VII Simpósio de Geologia da Amazônia; CD-ROM, Belém: Sociedade Brasileira de Geologia, Núcleo Norte*.

Burruss R. C. and Laughrey C. D. (2010) Carbon and hydrogen isotopic reversals in deep basin gas: Evidence for limits to the stability of hydrocarbons. *Org. Geochem.* **41**(12), 1285-1296.

Burruss R. C. and Ryder R. T. (2003) Composition of Crude Oil and Natural Gas Produced from 14 Wells in the Lower Silurian" Clinton" Sandstone and Medina Group, Northeastern Ohio and Northwestern Pennsylvania. US Department of the Interior, US Geological Survey.

Campos J. N. P., Murakami C. Y., Mauro Filho A., Barbosa Filho C. M. (1991) Evolução tectono-sedimentar, habitat do petróleo e exploração da Bacia do Solimões, Petrobras Internal Report, SIEX n° 131-08015, 28 p., Petrobras, Belém, Brazil.

Caputo M. V. and Silva O. B. (1990) Sedimentação e tectônica da Bacia do Solimões. In: Origem e Evolução de Bacias Sedimentares, Gabaglia, G.P.R. and Milani, E.J. (eds.) Petróleo Brasileiro S/A, Rio de Janeiro, RJ, Brazil, p. 169-193.

Carignan J., Hild P., Mevelle G., Morel J. and Yeghicheyan D. (2001) Routine analyses of trace elements in geological samples using flow injection and low pressure on-line liquid chromatography coupled to ICP-MS: a study of geochemical reference materials BR, DR-N, UB-N, AN-G and GH. *Geostandard. Newslett.* **25**(2-3), 187–198.

Charlou J. L., Donval J. P., Fouquet Y., Jean-Baptiste P. and Holm N. (2002) Geochemistry of high H_2 and CH_4 vent fluids issuing from ultramafic rocks at the Rainbow hydrothermal field (36°14′N, MAR). *Chem. Geol.* **191**(4), 345-359.

Clayton C. (1991) Carbon isotope fractionation during natural gas generation from kerogen. *Mar. Petrol. Geol.* **8**(2), 232-240.

Dai J., Xia X., Qin S. and Zhao J. (2004) Origins of partially reversed alkane $\delta^{13}C$ values for biogenic gases in China. *Org. Geochem.* **35**(4), 405-411.

Dai J., Li J., Luo X., Zhang W., Hu G., Ma C., ... and Ge S. (2005) Stable carbon isotope compositions and source rock geochemistry of the giant gas accumulations in the Ordos Basin, China. *Org. Geochem.* **36**(12), 1617-1635.

Dai J., Zou C., Zhang S., Li J., Ni Y., Hu G., ... and Ma C. (2008) Discrimination of abiogenic and biogenic alkane gases. *Science in China Series D: Earth Sciences*, **51**(12), 1737-1749.

Daval D., Sissmann O., Menguy N., Saldi G. D., Guyot F., Martinez I., ... and Hellmann, R. (2011) Influence of amorphous silica layer formation on the dissolution rate of olivine at 90°C and elevated pCO_2. *Chem. Geol.* **284**(1), 193-209.

Des Marais D. J., Donchin, J. H., Nehring N. L. and Truesdell A. H. (1981) Molecular carbon isotopic evidence for the origin of geothermal hydrocarbons. *Nature* **292,** 826-828.

Eiras J. F. (1998a) Tectonics, sedimentation and petroleum system of the Solimões Basin, Amazon State. In: Torre, A. J. and Associates (eds.) Searching for oil and gas in the land of giants. Schlumberger, The Search, Special Edition on Brazil, p. 23-31. Rio de Janeiro.

Eiras J. F., Becker C. R., Souza E. M., Gonzaga F. G., da Silva J. G. F., Daniel L. M. F., Matsuda N. S. and Feijo F. J. (1994) Bacia do Solimoes: Boletim de Geociencias da Petrobras, Rio de Janeiro, **8**(1), 17-45.

Elias A. R. D., De Ros L. F., Mizusaki A. M. P. and Anjos S. M. C. (2004) Diagenetic patterns in eolian/coastal sabkha reservoirs of the Solimões basin, northern brazil. *Sediment. Geol.* **169**(3-4), 191-217.

Elias A. D., De Ros L. F., Mizusaki A. M. and Kawashita K. (2007) Isotopic evidence on the diagenetic evolution of coastal sabkha reservoirs from the Solimões Basin, northern Brazil. *Gondwana Research*, **11**(4), 553-567.

Etiope G., Schoell M. and Hosgörmez, H. (2011) Abiotic methane flux from the Chimaera seep and Tekirova ophiolites (Turkey): understanding gas exhalation from low temperature serpentinization and implications for Mars. *Earth Planet. Sc. Lett.* **310**(1), 96-104.

Figueiredo A. M. F. and Milani E. J. (2000) Petroleum systems of South American basins. In: Tectonic Evolution of South America, Cordani, U. G. Milani, E. J., ThomazFilho, A., Campos, D. A. (eds.), pp. 689-718, 31st International Geological Congress, August, 2000, Rio de Janeiro, RJ, Brazil.

Foustoukos D. I. and Seyfried W. E. (2004) Hydrocarbons in hydrothermal vent fluids: the role of chromium-bearing catalysts. *Science*, **304**(5673), 1002-1005.

Freitas L.C.S., Cerqueira J.R. and Barbanti S.M. (2000) Diamondoids as indicators of oil cracking in the Juruá sub-basin, Solimões Basin, Northern Brazil. In: Proceedings of the 7th Latin-American Congress on Organic Geochemistry (ALAGO), New Perspectives on

Organic Geochemistry for the Third Millennium, 22-26-October-2000, Foz de Iguaçu, PR, Brazil, Trindade, L. A. F., Macedo, A. C., Barbanti, S. M. (eds.), p. 33-34.

Fu Q., Sherwood Lollar B., Horita J., Lacrampe-Couloume G. and Seyfried, Jr., W. E. (2007) Abiotic formation of hydrocarbons under hydrothermal conditions: Constraints from chemical and isotope data. *Geochim. Cosmochim. Ac.* **71**(8), 1982-1998.

Giardini A. A., Salotti C. A. and Lakner J. F. (1968) Synthesis of graphite and hydrocarbons by reaction between calcite and hydrogen. *Science* **159**(3812), 317-319.

Gonzaga F. G., Gonalves F. T. T. and Coutinho L. F. C. (2000) Petroleum Geology of the Amazonas Basin, Brazil: Modeling of Hydrocarbon Generation and Migration, *AAPG Memoir* **73**, Chapter 13

Helgeson H. C., Delany J. M., Nesbitt H. W. and Bird D. K. (1978) Summary and critique of the thermodynamic properties of rock-forming minerals. *Am. J. Sci.* **278A**, 1-229.

Holloway J. R. (1984) Graphite-CH_4-H_2O-CO_2 equilibria at low-grade metamorphic conditions. *Geology* **12**(8), 455-458.

Holm N. G. and Charlou J. L. (2001) Initial indications of abiotic formation of hydrocarbons in the Rainbow ultramafic hydrothermal system, Mid-Atlantic Ridge. *Earth Planet. Sc. Lett.* **191**(1-2), 1-8.

Horita J. and Berndt M. E. (1999) Abiogenic methane formation and isotopic fractionation under hydrothermal conditions. *Science* **285**(5430), 1055-1057.

Hosgormez H., Etiope G. and Yalcin M. N. (2008) New evidence for a mixed inorganic and organic origin of the Olympic Chimaera fire (Turkey): a large onshore seepage of abiogenic gas. *Geofluids* **8**(4), 263-273.

Hu G., Ouyang Z., Wang X. and Wen Q. (1998) Carbon isotopic fractionation in the process of Fischer-Tropsch reaction in primitive solar nebula. *Sci. China Ser. D: Earth Sci.* **41**(2), 202-207.

Huang H., Yang J., Yang Y. and Du X. (2004) Geochemistry of natural gases in deep strata of the Songliao Basin, NE China. *Int. J. Coal Geol.* **58**(4), 231-244.

Hunkeler D., Jörger D., Häberli K., Höhener P. and Zeyer J. (1998) Petroleum hydrocarbon mineralization in anaerobic laboratory aquifer columns. *J. Contam. Hydrol.* **32**(1), 41-61.

James A. T. and Burns B. J. (1984) Microbial alteration of subsurface natural gas accumulations. *AAPG Bulletin* **68**(8), 957-960.

Jenden P. D., Drazan D. J. and Kaplan I. R. (1993) Mixing of thermogenic natural gases in northern Appalachian Basin. *AAPG Bulletin* **77**(6), 980-998.

Johnson J. W., Oelkers E. H. and Helgeson H. C. (1992) SUPCRT92: A software package for calculating the standard molal thermodynamic properties of minerals, gases, aqueous species, and reactions from 1 to 5000 bar and 0 to 1000°C. *Comput. Geosci.* **18**(7), 899-947.

Jones L. C., Rosenbauer R., Goldsmith J. I. and Oze C. (2010) Carbonate control of H_2 and CH_4 production in serpentinization systems at elevated P-Ts. *Geophys. Res. Lett.* **37**(14).

Katz B. J. (2011) Microbial processes and natural gas accumulations. *Open Geology Journal*, **5**, 75-83.

Kelley D. S., Karson J. A., Blackman D. K., FruÈh-Green G. L., Butterfield D. A., Lilley M. D., ... and Rivizzigno P. (2001) An off-axis hydrothermal vent field near the Mid-Atlantic Ridge at 30 N. *Nature* **412**(6843), 145-149.

Kharaka Y.K., Maest A.S., Carothers W.W., Law L.M., Lamothe P.J. and Fries T.L. (1987) Geochemistry of metal-rich brines from central Mississippi Slat Dome Basin, U.S.A. *Applied Geochemistry* **2**, 543-561.

Krouse H. R., Viau C. A., Eliuk L. S., Ueda A. and Halas S. (1988) Chemical and isotopic evidence of thermochemical sulphate reduction by light hydrocarbon gases in deep carbonate reservoirs. *Nature* **333**, 415-419.

Larin N., Zgonnik V., Rodina S., Deville E., Prinzhofer A. and Larin V. N. (2014) Natural molecular hydrogen seepage associated with surficial, rounded depressions on the European craton in Russia. *Natural Resources Research*, 1-15.

Laughrey C. D. and Baldassare F. J. (1998) Geochemistry and origin of some natural gases in the Plateau Province, central Appalachian Basin, Pennsylvania and Ohio. *AAPG bulletin* **82**(2), 317-335.

Lebeau O., Busigny V., Chaduteau C. and Ader M. (2014) Organic matter removal for the analysis of carbon and oxygen isotope compositions of siderite. *Chem. Geol.* **372**, 54-61.

Malvoisin B., Carlut J. and Brunet F. (2012) Serpentinization of oceanic peridotites: 1. A high-sensitivity method to monitor magnetite production in hydrothermal experiments. *J. Geophys. Res.-Sol. Ea. (1978–2012)*, **117**(B1).

McCollom T. M. (2003) Formation of meteorite hydrocarbons from thermal decomposition of siderite ($FeCO_3$). *Geochim. Cosmochim. Ac.* **67**(2), 311-317.

McCollom T. M. (2013) Laboratory simulations of abiotic hydrocarbon formation in Earth's deep subsurface. In: *Carbon in Earth* (eds. R.M. Hazen, A.P. Jones, J.A. Baross), *Rev. Mineral. Geochem.* **75**, pp. 467-494. Mineralogical Society of America.

McCollom T. M. and Seewald J. S. (2006) Carbon isotope composition of organic compounds produced by abiotic synthesis under hydrothermal conditions. *Earth Planet. Sc. Lett.* **243**(1), 74-84.

McCollom T. M., Lollar B. S., Lacrampe-Couloume G. and Seewald, J. S. (2010) The influence of carbon source on abiotic organic synthesis and carbon isotope fractionation under hydrothermal conditions. *Geochim. Cosmochim. Ac.* **74**(9), 2717-2740.

Mello M. R., Koutsoukos E. A. M., Mohriak W. U. and Bacoccoli G. (1994) Selected petroleum systems in Brazil. In: Maggon L. B. and W. G. Dow (eds.). *The petroleum system – from source to trap*. AAPG, Tulsa, Memoir, **60**, 499-512.

Milesi V., Guyot F., Brunet F., Richard L., Recham N., Benedetti M. and Prinzhofer A. (2015) Formation of CO_2, H_2 and condensed carbon from siderite dissolution in the 200–300°C range and at 50MPa. *Geochim. Cosmochim. Ac.*, **154**, 201-211.

Mosmann R., Falkenhein F. U. H., Gonçalves A., Nepomuceno Filho F. (1987) Oil and gás potential of the Amazon Paleozoic basins. AAPG Memoir #**27**, 207-241.

Murakami C. Y., Gonçalves F. T. T., Eiras J. F., Becker C. R., Lima M. P., and Daniel L. M. F. (1993) Habitat of petroleum in the Solimões Basin, Brazil. In: 3rd Latin-American Congress on Organic Geochemistry (ALAGO), Extended Abstracts, Mello, M. R. and Trindade, L. A. F. (eds.), 113-115.

Newell K. D., Doveton J. H., Merriam D. F., Lollar B. S., Waggoner W. M. and Magnuson L. M. (2007) H_2-rich and hydrocarbon gas recovered in a deep Precambrian well in northeastern Kansas. *Natural Resources Research*, **16**(3), 277-292.

Perry, Jr., E. C. and Ahmad S. N. (1977) Carbon isotope composition of graphite and carbonate minerals from 3.8-AE metamorphosed sediments, Isukasia, Greenland. *Earth Planet. Sc. Lett.* **36**(2), 280-284.

Pillot D., Deville E. and Prinzhofer A. (2013) Identification and Quantification of Carbonate Species Using Rock-Eval Pyrolysis. *Oil & Gas Science and Technology – Rev. IFP Energies nouvelles*, **69**(2), 341-349.

Prinzhofer A. A. and Huc A. Y. (1995) Genetic and post-genetic molecular and isotopic fractionations in natural gases. *Chem. Geol.* **126**(3), 281-290.

Proskurowski G., Lilley M. D., Seewald J. S., Früh-Green G. L., Olson E. J., Lupton J. E., Sylva S. P. and Kelley D. S. (2008) Abiogenic hydrocarbon production at Lost City hydrothermal field. *Science* **319**(8563), 604-607.

Rodrigues R., Triguis J. A., Araújo C. V. and Brazil I. R. (1990) Geoquímica e faciologia orgânica dos sedimentos da Bacia do Solimões. PETROBRAS/CENPES/DEPEX, Internal Report, p. 115.

Saldi G. D., Daval D., Morvan G. and Knauss K. G. (2013) The role of Fe and redox conditions in olivine carbonation rates: an experimental study of the rate limiting reactions at 90 and 150°C in open and closed systems. *Geochim. Cosmochim. Ac.* **118**, 157-183.

Schidlowski M. (2001) Carbon isotopes as biogeochemical recorders of life over 3.8 Ga of Earth history: evolution of a concept. *Precambrian Res.* **106**(1), 117-134.

Sherwood Lollar B., Westgate T. D., Ward J. A., Slater G. F., and Lacrampe-Couloume G. (2002) Abiogenic formation of alkanes in the earth's crust as a minor source for global hydrocarbon reservoirs. *Nature* **416**(6880), 522-524.

Sherwood Lollar B., Lacrampe-Couloume G., Slater G. F., Ward J., Moser D. P., Gihring T. M., ... and Onstott T. C. (2006) Unravelling abiogenic and biogenic sources of methane in the Earth's deep subsurface. *Chem. Geol.* **226**(3), 328-339.

Shock E. L. and Helgeson H. C. (1988) Calculation of the thermodynamic and transport properties of aqueous species at high pressure and temperatures: Correlation algorithms for ionic species and equation of state predictions to 5 kb and 1000°C *Geochim. Cosmochim. Ac.* **52**, 2009-2036.

Shock E. L., Helgeson H. C. and Sverjensky D. A. (1989) Calculation of the thermodynamic and transport properties of aqueous species at high pressures and temperatures: Standard partial molal properties of inorganic neutral species. *Geochim. Cosmochim. Ac.* **53**, 2157-2183.

Shock E. L., Sassani D. C., Willis M., and Sverjensky D. A. (1997) Inorganic species in geologic fluids: Correlations among standard molal thermodynamic properties of aqueous ions and hydroxide complexes. *Geochim. Cosmochim. Ac.* **61**, 907-950.

Sissmann O., Daval D., Brunet F., Guyot F., Verlaguet A., Pinquier Y., ... and Martinez I. (2013) The deleterious effect of secondary phases on olivine carbonation yield: Insight from time-resolved aqueous-fluid sampling and FIB-TEM characterization. *Chem. Geol.* **357**, 186-202.

Steele A., McCubbin F. M., Fries M. D., Golden D. C., Ming D. W. and Benning L. G. (2012) Graphite in the Martian meteorite Allan Hills 84001. *Am. Mineral.* **97**(7), 1256-1259.

Tang Y. and Xia X. (2010) Kinetics and mechanism of shale-gas formation: a quantitative interpretation of gas isotope "rollover" for shale gas formation. In : *AAPG Hedberg Conf.* pp. 5-10.

Taran Y. A., Kliger G. A. and Sevastianov V. S. (2007) Carbon isotope effects in the open-system Fischer–Tropsch synthesis. *Geochim. Cosmochim. Ac.* **71**(18), 4474-4487.

Tissot B. P., Pelet R. and Ungerer P. H. (1987) Thermal history of sedimentary basins, maturation indices, and kinetics of oil and gas generation. *AAPG bulletin* **71**(12), 1445-1466.

Ueno Y., Yurimoto H., Yoshioka H., Komiya T. and Maruyama S. (2002) Ion microprobe analysis of graphite from ca. 3.8 Ga metasediments, Isua supracrustal belt, West Greenland: Relationship between metamorphism and carbon isotopic composition. *Geochim. Cosmochim. Ac.* **66**(7), 1257-1268.

van Zuilen M. A., Lepland A., Teranes J., Finarelli J., Wahlen M. and Arrhenius G. (2003) Graphite and carbonates in the 3.8 Ga old Isua Supracrustal Belt, southern West Greenland. *Precambrian Res.* **126**(3-4), 331-348.

Whiticar M. J., Faber E. and Schoell M. (1986). Biogenic methane formation in marine and freshwater environments: CO_2 reduction vs. acetate fermentation – isotope evidence. *Geochim. Cosmochim. Ac.* **50**(5), 693-709.

Xia X., Chen J., Braun R. and Tang Y. (2013) Isotopic reversals with respect to maturity trends due to mixing of primary and secondary products in source rocks. *Chem. Geol.* **339**, 205-212.

Yuen G., Blair N., Des Marais D. J. and Chang, S. (1984) Carbon isotope composition of low molecular weight hydrocarbons and monocarboxylic acids from Murchison meteorite. *Nature* **307**, 252-254.

Zolotov M. Y. and Shock E. L. (2000) An abiotic origin for hydrocarbons in the Allan Hills 84001 Martian meteorite through cooling of magmatic and impact-generated gases. *Meteorit. Planet. Sci.* **35**(3), 629-638.

Zumberge J., Kevin Ferworn K. and Brown S. (2012) Isotopic reversal ('rollover') in shale gases produced from the Mississippian Barnett and Fayetteville formations. *Mar. Petrol. Geol.* **31**(1), 43-52.

Figure 1

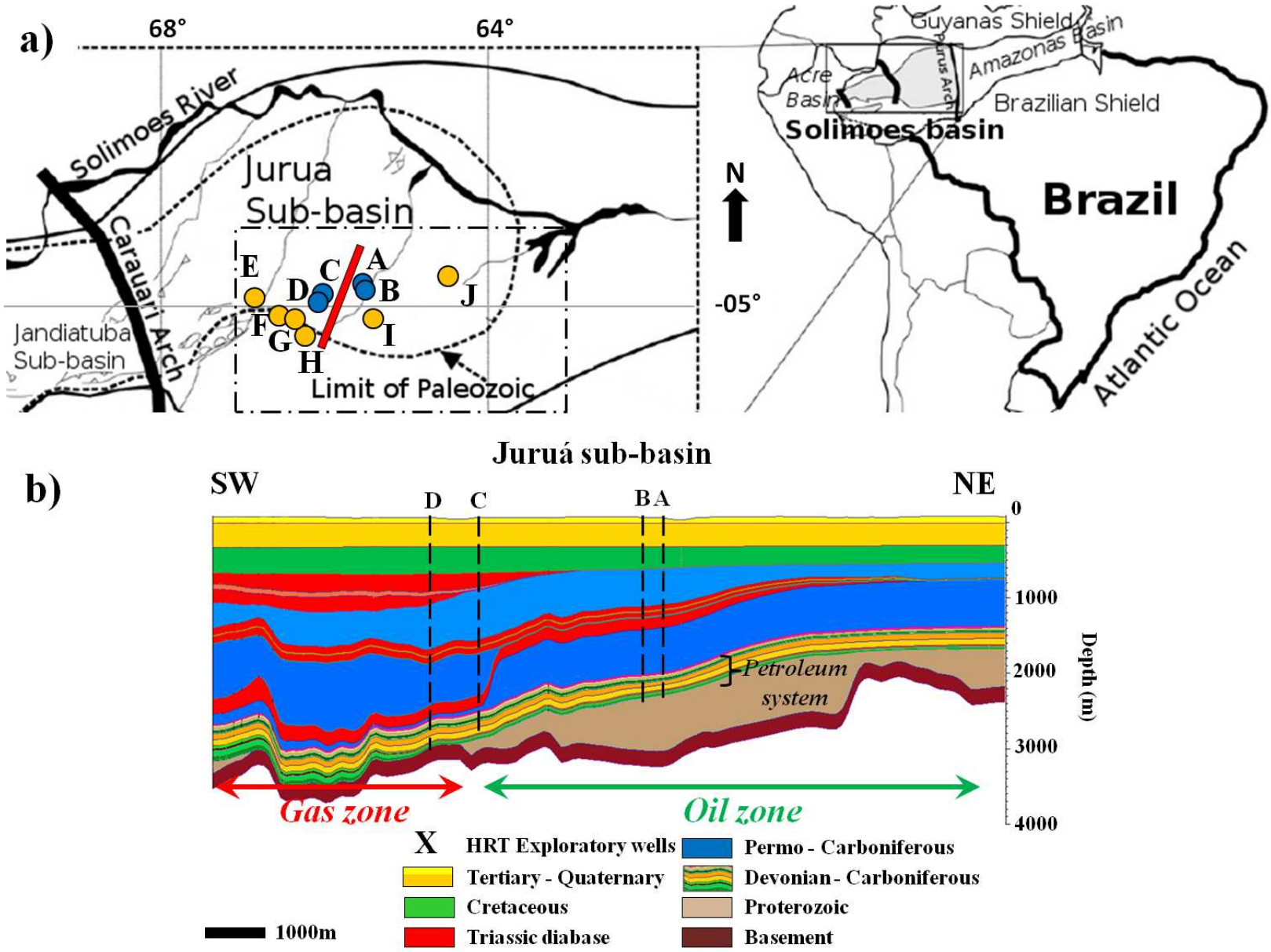
a)
68°
64°
Solimoes River
Jurua
Sub-basin
Carauari Arch
Jandiatuba
Sub-basin
E
D
C
A
B
J
F
G
H
I
Limit of Paleozoic
N
-05°
Guyanas Shield
Amazonas Basin
Purus Arch
Acre
Basin
Brazilian Shield
Solimoes basin
Brazil
Atlantic Ocean
b)
Juruá sub-basin
SW
NE
D
C
B
A
0
1000
2000
3000
4000
Depth (m)
Petroleum
system
Gas zone
Oil zone
X
HRT Exploratory wells
Tertiary - Quaternary
Cretaceous
Triassic diabase
Permo - Carboniferous
Devonian - Carboniferous
Proterozoic
Basement
1000m

Figure 2

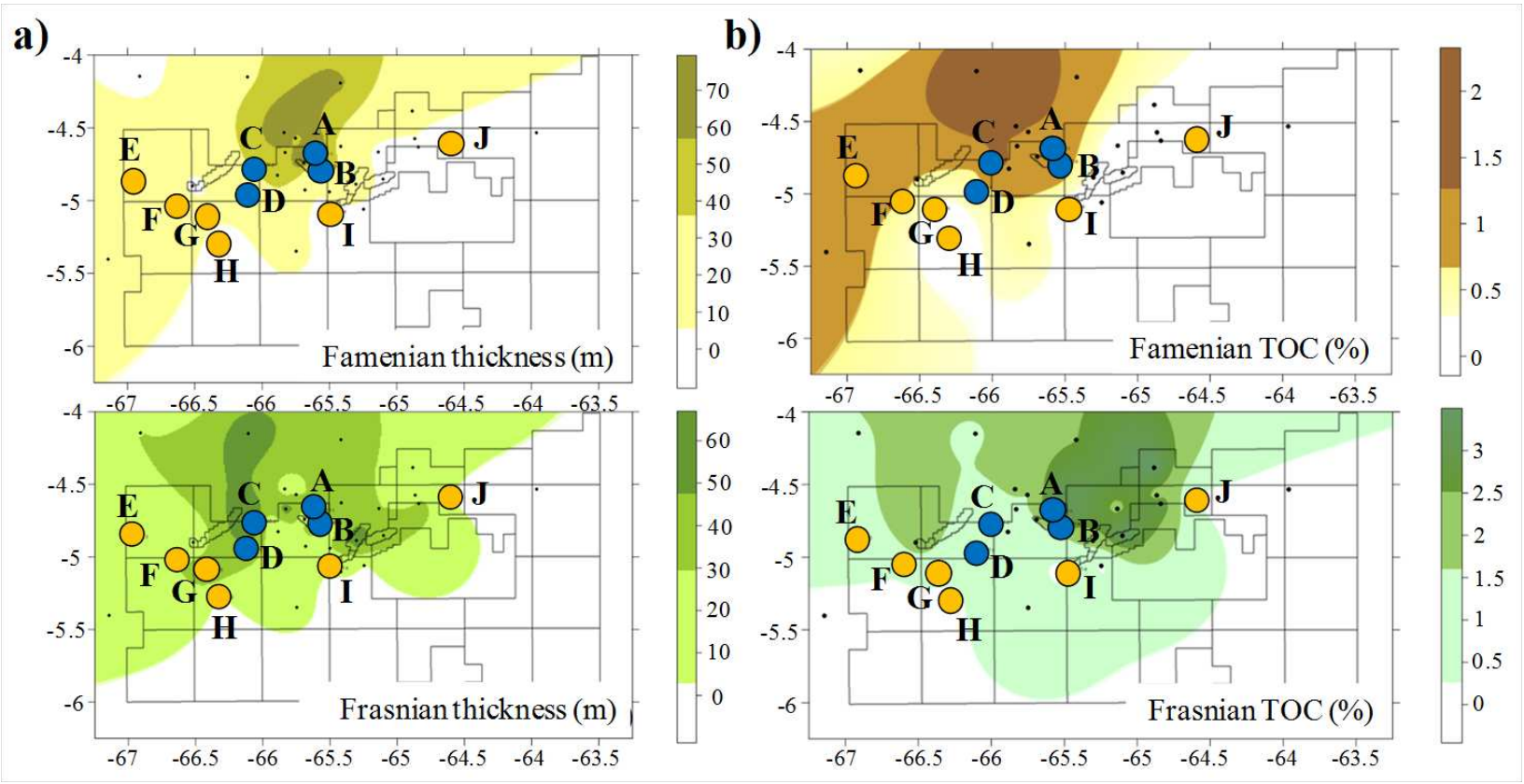
a)
b)
A
B
C
D
E
F
G
H
I
J
Famenian thickness (m)
Famenian TOC (%)
Frasnian thickness (m)
Frasnian TOC (%)
-4
-4.5
-5
-5.5
-6
-67
-66.5
-66
-65.5
-65
-64.5
-64
-63.5
70
60
50
40
30
20
10
0
2
1.5
1
0.5
0
3
2.5
2

Figure 3

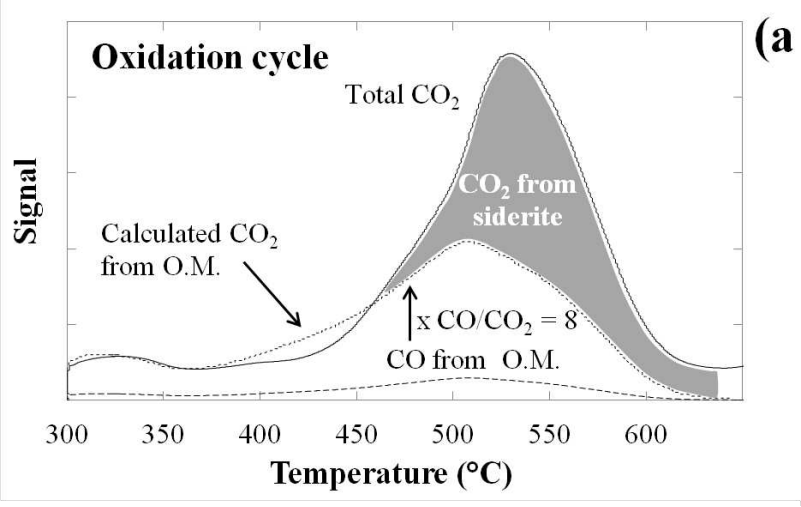
Oxidation cycle
Total CO_2
CO_2 from siderite
Calculated CO_2 from O.M.
x CO/CO_2 = 8
CO from O.M.
Signal
300
350
400
450
500
550
600
Temperature (°C)
(a

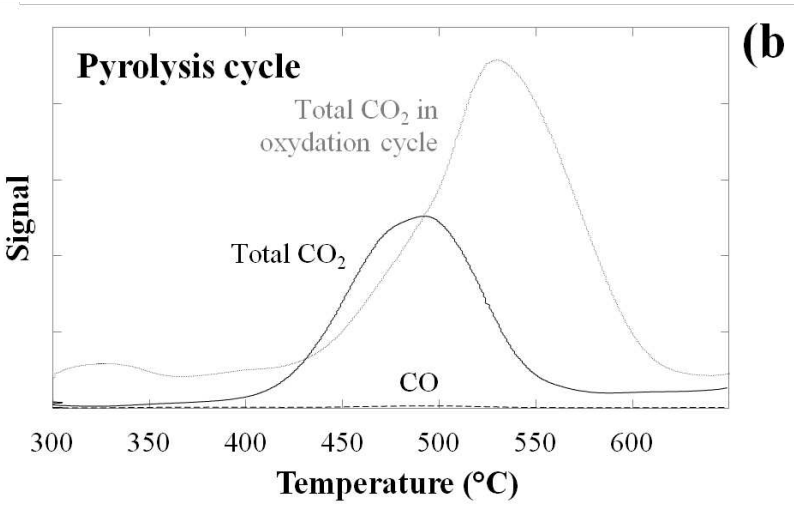
Pyrolysis cycle
Total CO_2 in oxydation cycle
Total CO_2
CO
Signal
300
350
400
450
500
550
600
Temperature (°C)
(b

Figure 4

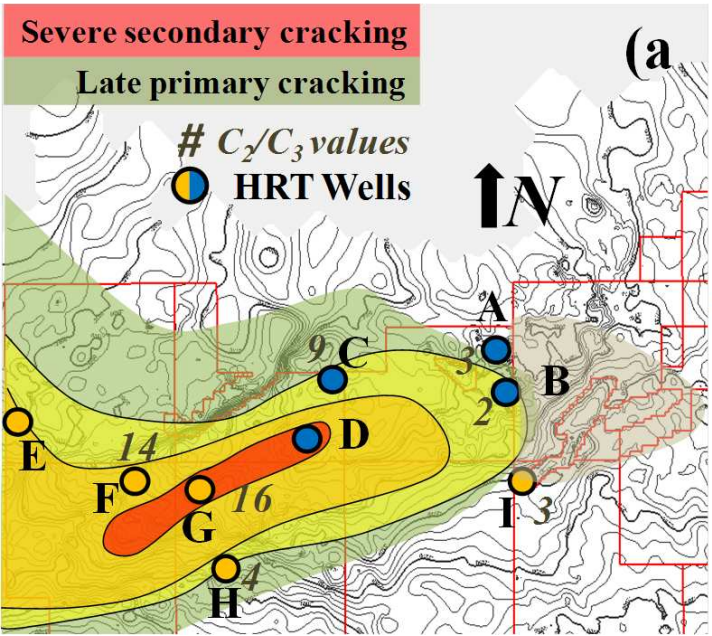
Severe secondary cracking
Late primary cracking
C_2/C_3 values
HRT Wells
N
(a
A
B
C
D
E
F
G
H
I
9
3
2
14
16
4
3

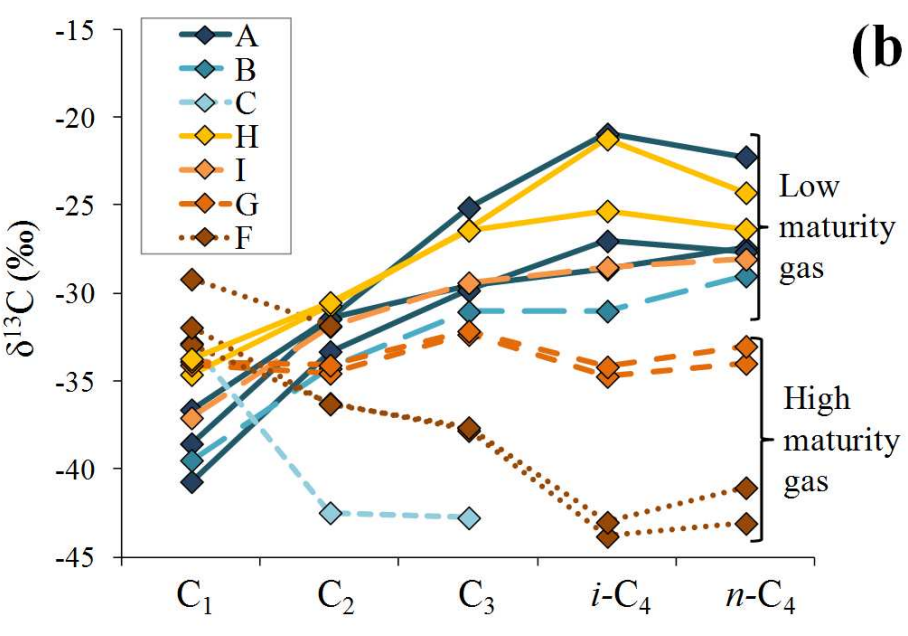
(b
A
B
C
H
I
G
F
-15
-20
-25
-30
-35
-40
-45
$\delta^{13}C$ (‰)
C_1
C_2
C_3
i-C_4
n-C_4
Low maturity gas
High maturity gas

Figure 5

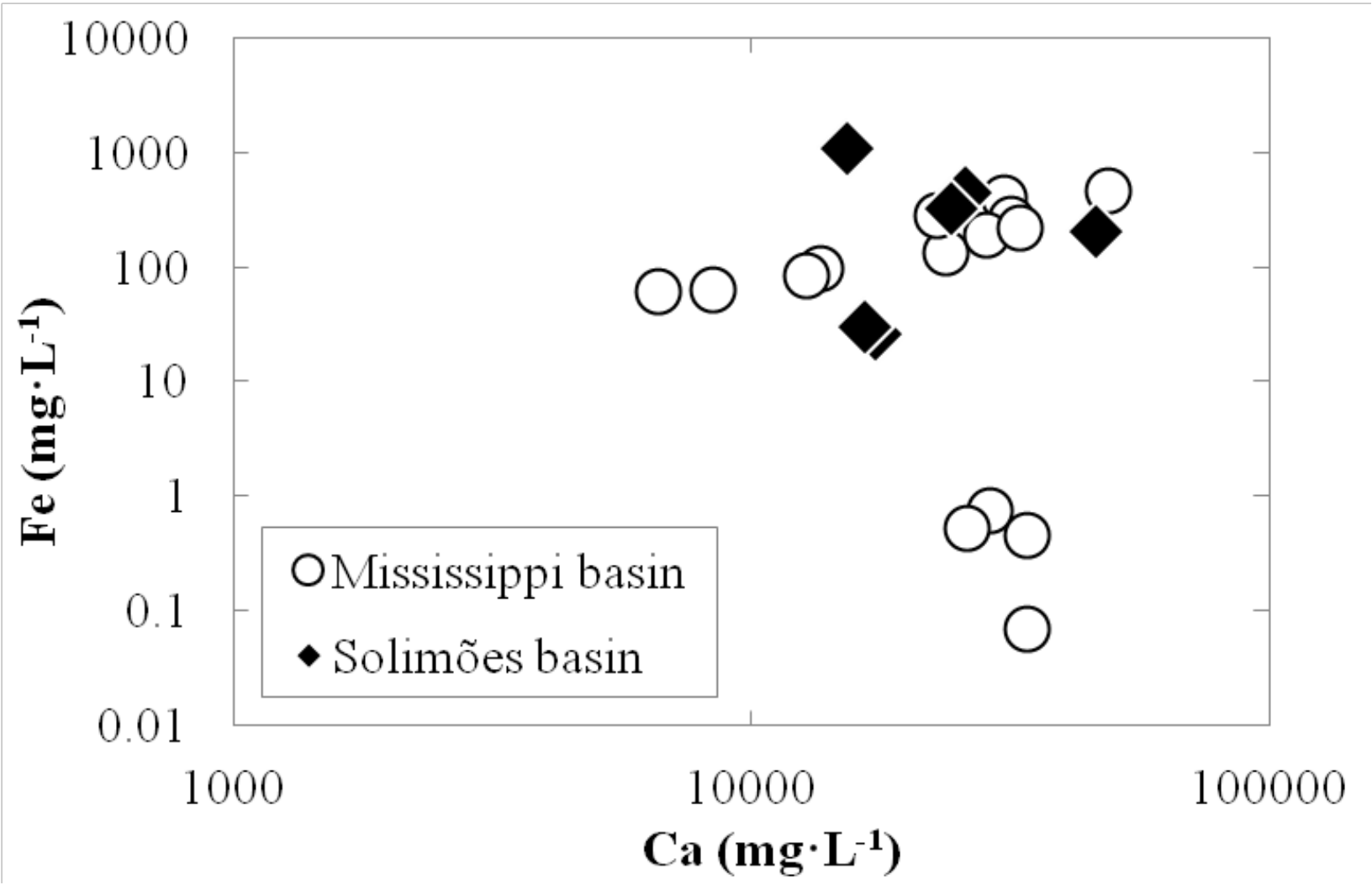
10000
1000
100
10
1
0.1
0.01
Fe (mg·L-1)
Mississippi basin
Solimões basin
1000
10000
100000
Ca (mg·L-1)

Figure 6

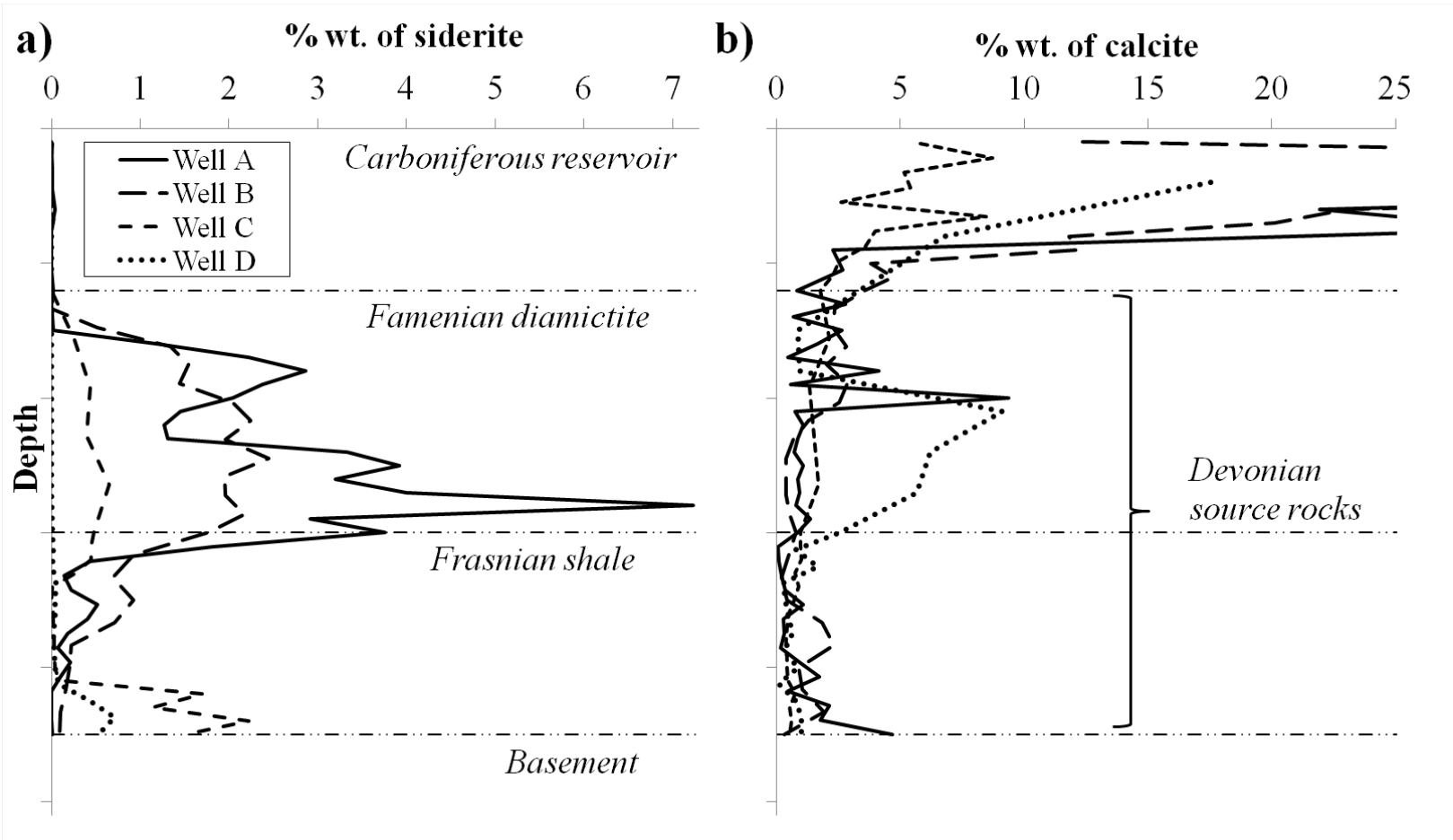
a)
% wt. of siderite
0
1
2
3
4
5
6
7
Well A
Well B
Well C
Well D
Carboniferous reservoir
Famenian diamictite
Depth
Frasnian shale
Basement
b)
% wt. of calcite
0
5
10
15
20
25
Devonian
source rocks

Figure 7

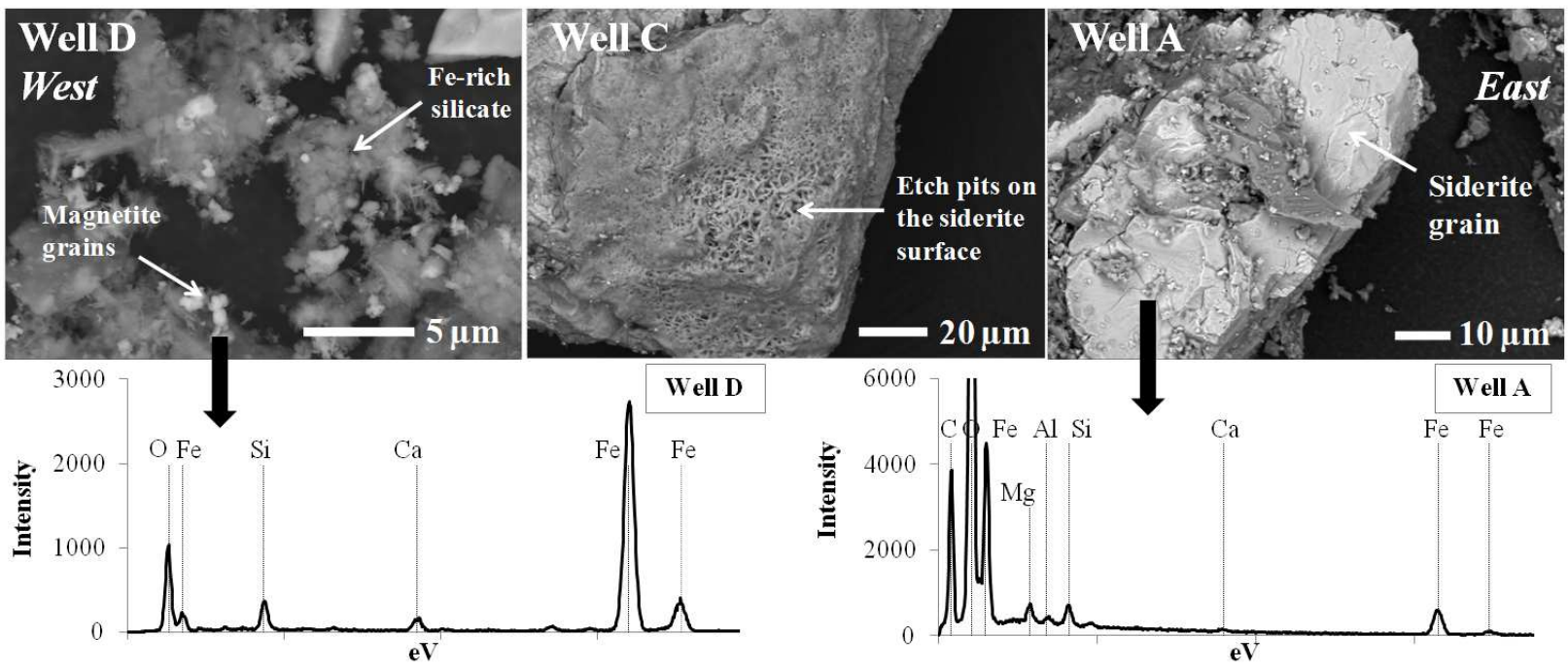
Well D
West
Fe-rich silicate
Magnetite grains
5 µm
Well C
Etch pits on the siderite surface
20 µm
Well A
East
Siderite grain
10 µm
Well D
Intensity
3000
2000
1000
0
O Fe
Si
Ca
Fe
Fe
eV
Well A
Intensity
6000
4000
2000
0
C O Fe Al Si
Mg
Ca
Fe Fe
eV

Figure 8

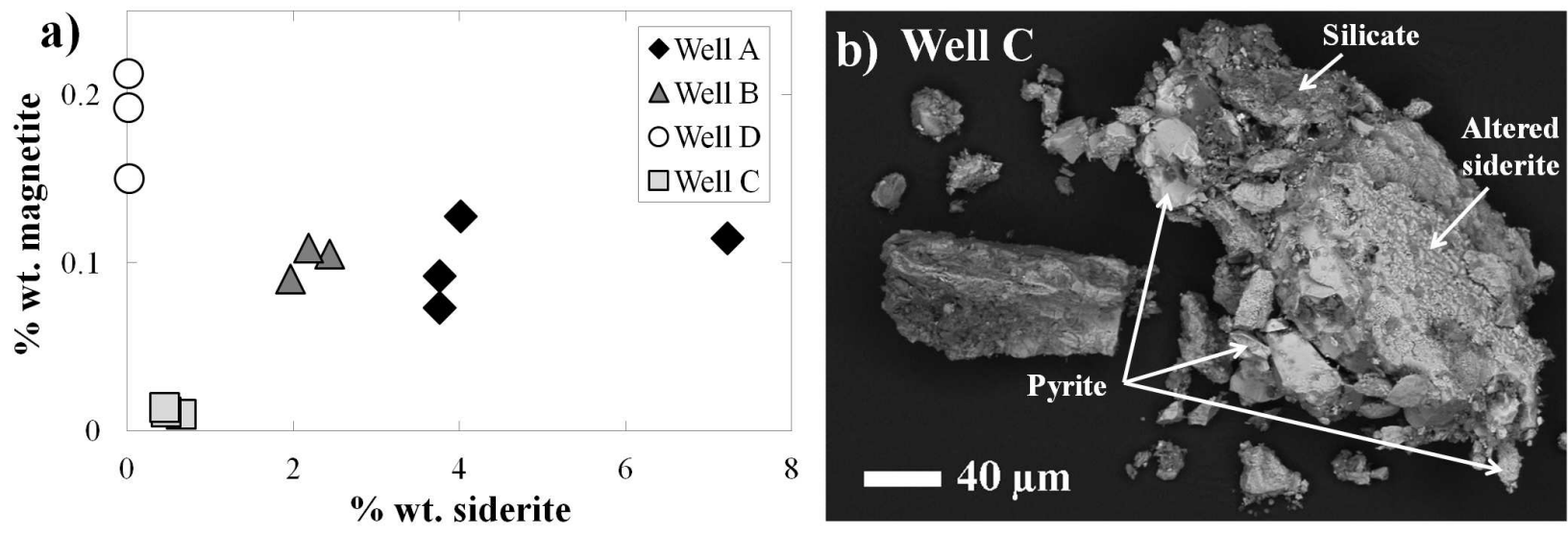
a)
Well A
Well B
Well D
Well C
% wt. magnetite
0.2
0.1
0
0
2
4
6
8
% wt. siderite
b) Well C
Silicate
Altered siderite
Pyrite
40 µm

Figure 9

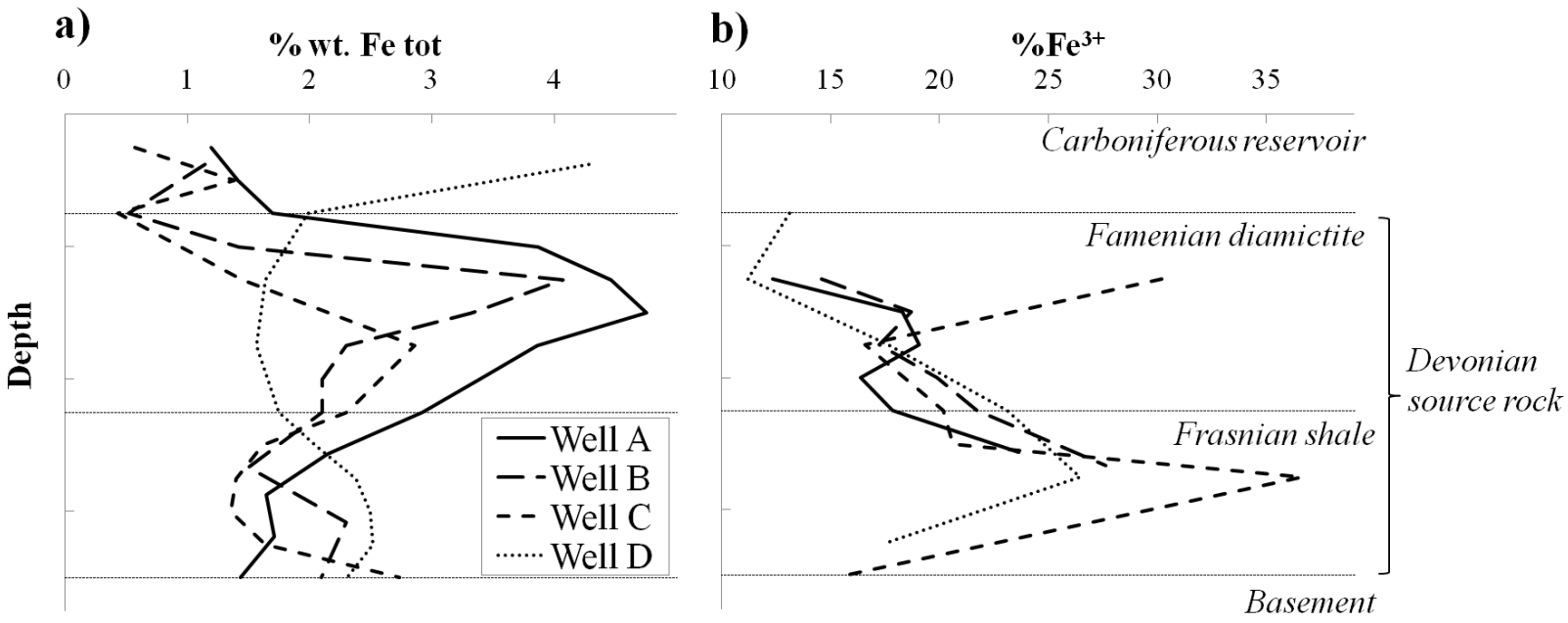
a)
% wt. Fe tot
0
1
2
3
4
Depth
Well A
Well B
Well C
Well D
b)
%Fe3+
10
15
20
25
30
35
Carboniferous reservoir
Famenian diamictite
Frasnian shale
Devonian source rock
Basement

Figure 10

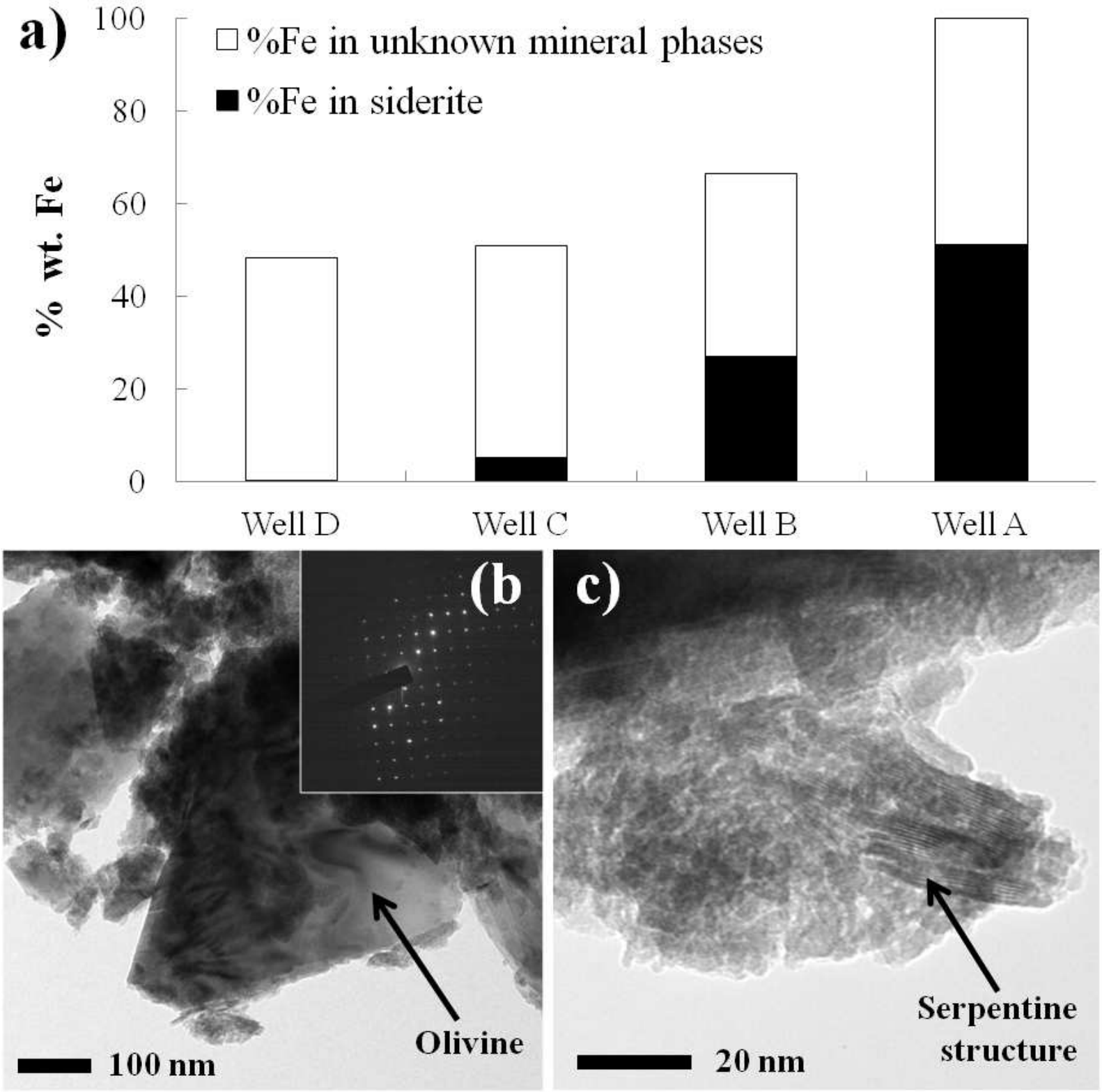
a)
100
80
60
40
20
0
% wt. Fe
%Fe in unknown mineral phases
%Fe in siderite
Well D
Well C
Well B
Well A
(b
Olivine
100 nm
c)
Serpentine
structure
20 nm

Figure 11

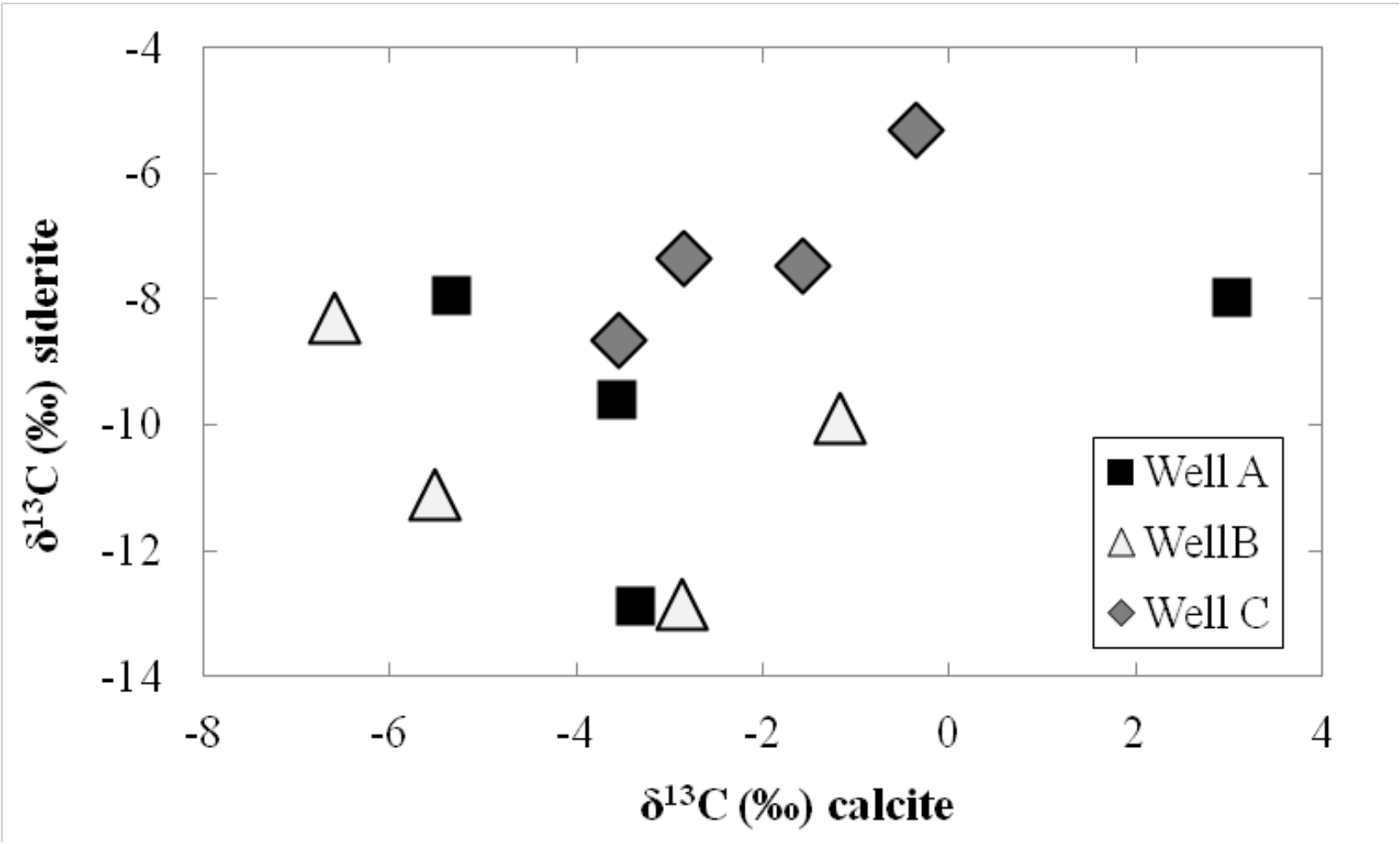
-4
-6
-8
-10
-12
-14
-8
-6
-4
-2
0
2
4
δ13C (‰) siderite
δ13C (‰) calcite
Well A
WellB
Well C

Figure 12

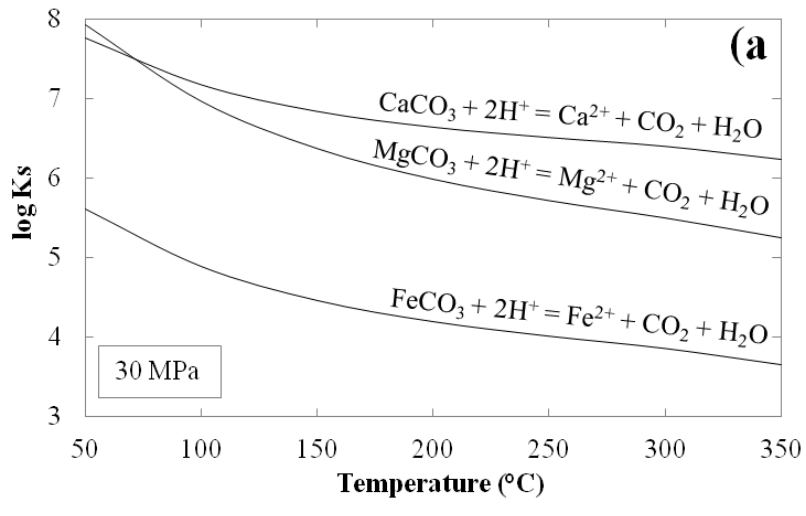
(a)
30 MPa
$CaCO_3 + 2H^+ = Ca^{2+} + CO_2 + H_2O$
$MgCO_3 + 2H^+ = Mg^{2+} + CO_2 + H_2O$
$FeCO_3 + 2H^+ = Fe^{2+} + CO_2 + H_2O$
log Ks
Temperature (°C)
8
7
6
5
4
3
50
100
150
200
250
300
350

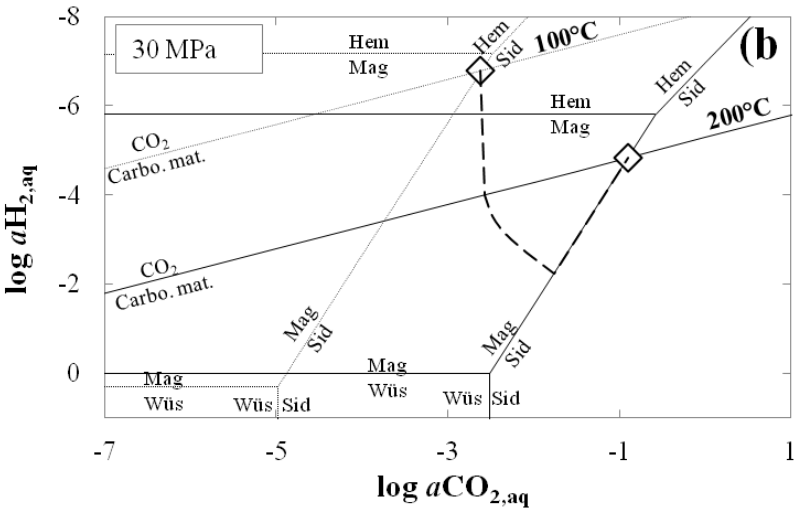
(b)
30 MPa
Hem
Mag
Hem
Sid
100°C
Hem
Mag
Hem
Sid
200°C
CO_2
Carbo. mat.
CO_2
Carbo. mat.
Mag
Sid
Mag
Sid
Mag
Wüs
Wüs
Sid
Mag
Wüs
Wüs
Sid
log $aH_{2,aq}$
log $aCO_{2,aq}$
-8
-6
-4
-2
0
-7
-5
-3
-1
1

CAPTIONS

Fig. 1 Regional geologic setting of the Solimões basin; (a) geographic location (modified from Elias *et al.*, 2004) of the exploratory wells of the HRT Oil and Gas Company. The blue dots represent Well A, B, C and D, for which the mineral composition of the source rock was specifically studied. The red line represents the location of the east-west geological section across the Juruá sub-basin (b) (modified from Eiras *et al.*, 1994). The dashed – dotted black box is the area shown in Fig. 2.

Fig. 2 Maps of the thickness (a) and the TOC content (b) of the Famenian and Frasnian source rocks.

Fig. 3 Diagrams illustrating the methodology to quantify the amount of siderite in rock samples with the Rock-Eval instrument using (a) the oxidation cycle, or (b) the pyrolysis cycle. In oxidation cycle, the CO_2 released from the organic matter disturbs the signal from the iron carbonate. In the case of highly mature organic matter, the use of pyrolysis cycle yields negligible the CO_2 from the organic matter so that the measured CO_2 derives only from the siderite decarbonation.

Fig. 4 Map of the distribution of the hydrocarbon gas maturity in the Solimões basin (a) and natural gas plot representing the carbon isotopic composition of methane to iso- and normal-butane depending on the number of carbon atoms for hydrocarbon gases of different drilling wells (b). Precision for $\delta^{13}C$ is less than or equal to the symbol size. In the map of gas

maturity (a), areas from green to red represent an increase of the gas maturity based on the C_2/C_3 ratio (brown numbers).

Fig. 5 Iron plotted against calcium concentrations of formation waters from the Solimões basin after correction for the contamination by drilling mud (closed diamonds). Concentrations reported by Kharaka *et al.*, (1987) in the brines of the Central Mississippi Salt Dome Basin are shown for comparison (open circles). Error bars are less or equal to the symbol size.

Fig. 6 Cross section analyses from the Carboniferous reservoir rocks to the Devonian source rocks of siderite (a) and calcite (b) contents quantified with the Rock-Eval instrument in Well A, B, C and D.

Fig. 7 SEM images in backscattered electron mode and EDX patterns of rock samples from the Famenian diamictite of Well A, C and D. In Well A, the EDX pattern is consistent with siderite. In Well D, the presence of iron and oxygen and the absence of carbon in the EDX pattern of the small and light grains are consistent with iron oxide.

Fig. 8 Magnetite plotted against siderite content in wt.% of selected rock samples of the Famenian diamictite from Well A, B, C and D (a), and SEM image in backscattered electron mode of rock sample from the Famenian diamictite of Well C showing pyrite associated with siderite (b).

Fig. 9 Cross section analyses from the Carboniferous reservoir rock to the Devonian source rocks of total iron content (a) and percentage of ferric iron among total iron (b) in Well A, B, C and D.

Fig. 10 Iron mass balance based on selected samples from the Famenian diamictite of Well A, B, C and D (a) and TEM observation of a sample from the Famenan diamictite of Well D (b and c). The iron mass balance is based on average values of four samples representative of the Famenian diamictite of each well. The amount of iron contained in siderite is calculated considering the siderite content from the Rock-Eval analyses and a stochiometric siderite ($FeCO_3$). The total amount of iron in each well is normalized to the one of the well with the highest iron content, i.e., Well A.

Fig. 11 Carbon isotopic compositions of siderite plotted against carbon isotopic compositions of calcite in samples from the Famenian diamictite of Well A, B and C. Error bars are less or equal to the symbol size.

Fig. 12 Diagram showing the equilibrium constant at 30 MPa of the reaction of dissolution of calcite, magnesite and siderite depending on the temperature (a), and H_2 – CO_2 activity diagram showing the stability domain of hematite, magnetite, wüstite, siderite and graphite at 50 MPa, 100°C (dotted lines) and 200°C (full lines) (b). In addition, a compositional path represents the evolution of the fluid composition following an increase of temperature from 100 to 200°C (dashed line) (see text for further details).

Table 1

Table 1. Molecular compositions of Solimões gases and stable carbon isotopic compositions of hydrocarbon gases

Well	Depth (m)	He	H_2	CO_2	N_2	C_1	C_2	C_3	*i*-C_4	*n*-C_4	C_2/C_3	$\delta^{13}C_1$	$\delta^{13}C_2$	$\delta^{13}C_3$	δ^{13}*i*-C_4	δ^{13}*n*-C_4
A	3096	-	-	-	-	87.32	7.69	2.87	0.45	0.93	2.68	-36.6	-31.5	-29.6	-28.6	-27.4
	3157	-	-	-	-	74.79	16.95	5.46	1.24	0.98	3.10	-38.6	-31.4	-25.1	-20.9	-22.2
	3195	-	-	-	-	69.93	17.04	8.15	1.25	2.30	2.09	-40.7	-33.3	-29.8	-27.0	-27.6
B	3290	0.11	6.92		1.3	57.55	16.91	11.79	1.60	3.77	1.43	-39.5	-34.3	-31.0	-31.0	-29.0
C	3356	-	-	-	-	97.15	2.45	0.28	0.04	0.04	8.66	-32.8	-42.5	-42.8	-	-
F	2762	0.28	0.01	0.4	3.0	94.90	1.33	0.10	0.010	0.008	13.85	-32.9	-36.3	-37.8	-43.8	-43.1
	2795	0.28	0.01	0.4	3.9	93.96	1.32	0.09	0.009	0.008	14.04	-31.9	-36.3	-37.6	-43.0	-41.1
	2887	0.10	3.20	1.4	11.8	82.02	1.39	0.10	0.010	0.013	13.76	-29.2	-31.8	-	-	-
G	2662	0.18	0.03	0.1	4.7	93.08	1.73	0.11	0.009	0.005	16.06	-33.9	-34.1	-32.2	-34.2	-33.0
	2686	0.21	0.01	0.1	8.3	89.60	1.68	0.11	0.009	0.006	15.26	-34.1	-34.6	-32.3	-34.7	-34.0
H	2259	0.81	0.00	0.2	24.3	70.31	3.078	0.910	0.1458	0.1692	3.38	-33.7	-30.5	-26.4	-25.3	-26.3
	2277	0.82	0.00	0.2	25.3	69.40	3.036	0.865	0.1294	0.1439	3.51	-34.6	-30.7	-26.4	-21.2	-24.3
I	2537	0.40	0.00	13.3	15.9	60.43	6.28	2.37	0.32	0.62	2.65	-37.1	-31.9	-29.4	-28.5	-28.1

The molecular composition is expressed in mol.% of the gas and the stable carbon isotopic composition in ‰ relative to the PDB standard. " - ": not analyzed.

Table 2

Table 2. Iron and calcium end-member concentrations of the Solimões formation waters

Well	Fe ($mg \cdot L^{-1}$)	Ca ($mg \cdot L^{-1}$)
A	452	25940
D	323	24180
E	1095	15280
F	205	46280
G	26	17380
I	30	16530

Table 3

Table 3. Carbon isotopic composition of siderite and calcite in the Famenian formation of the Solimões basin

Well	Depth (m)	$\delta^{13}C_{siderite}$	$\delta^{13}C_{calcite}$
A	3162	-8.0	3.0
	3183	-7.9	-5.3
	3201	-12.9	-3.4
	3207	-9.6	-3.6
B	3294	-11.1	-5.5
	3315	-8.3	-6.6
	3324	-12.8	-2.9
	3348	-9.9	-1.2
C	3198	-7.4	-2.8
	3207	-5.3	-0.3
	3216	-7.5	-1.6
	3240	-8.7	-3.5

The carbon isotopic composition is expressed in ‰ relative to the PDB standard.